

# The Medial Temporal Lobe Supports Visual Working Memory Precision

5 Weizhen Xie<sup>1,2\*</sup>, Marcus Cappiello<sup>2</sup>, John H. Wittig Jr.<sup>1</sup>, Srijan Bhasin<sup>1</sup>, Christopher Zawora<sup>1</sup>,  
Michael A. Yassa<sup>3</sup>, Edward Ester<sup>4</sup>, Sara K. Inati<sup>5</sup>, Kareem A. Zaghloul<sup>1\*†</sup>, Weiwei Zhang<sup>2\*†</sup>

## Affiliations:

10 <sup>1</sup>Surgical Neurology Branch, National Institute of Neurological Disorders and Stroke, National  
Institutes of Health, Bethesda MD

<sup>2</sup>Department of Psychology, University of California, Riverside

<sup>3</sup>Center for the Neurobiology of Learning and Memory, School of Biological Sciences,  
University of California, Irvine

<sup>4</sup>Department of Psychology, University of Nevada, Reno

15 <sup>5</sup>EEG Section, Office of the Clinical Director, National Institute of Neurological Disorders and  
Stroke, National Institutes of Health, Bethesda MD

20 \*Correspondence to: Weizhen Xie ([weizhen.xie@nih.gov](mailto:weizhen.xie@nih.gov), ORCID: 0000-0003-4655-6496),  
Kareem A. Zaghloul ([kareem.zaghloul@nih.gov](mailto:kareem.zaghloul@nih.gov), ORCID: 0000-0001-8575-3578), and Weiwei  
Zhang ([weiwei.zhang@ucr.edu](mailto:weiwei.zhang@ucr.edu), ORCID: 0000-0002-0431-5355).

†Senior authors contributed equally to this work and are listed in alphabetical order.

## Word Count

25 Abstract: 118

Main text: 1792

References and Notes: 418

Figure captions: 160 + 168 +120

30 Total: 2658

**Abstract:**

Precision of information retained in working memory (WM) underlies our ability to pinpoint the exact details of a stimulus that we recently encountered. However, it is unknown what mechanisms support WM precision. We hypothesize that WM precision relies on circuitry of the medial temporal lobe (MTL), a region commonly associated with the ability to distinguish similar information remembered in long-term memory. Using neuroimaging and intracranial recordings in human participants, we find that the MTL is sensitive to task demands on WM precision and retains precise item-level information during WM retention. Furthermore, perturbing the MTL through electrical stimulation or surgical removal markedly reduces WM precision. Collectively, our findings demonstrate that the MTL makes an essential contribution to WM precision.

**One Sentence Summary**

The medial temporal lobe supports the precision of visual working memory.

Working memory (WM) briefly retains a small amount of information to support ongoing mental processes (1). This core mental faculty is constrained by the precision of retained information (2–4) in addition to a limited storage capacity (5, 6). Reduced WM precision is often seen in aging (7, 8) and is associated with more variable memory recall errors (2–4). Although the neural substrates for WM capacity are well-documented (9–11), the mechanisms underlying WM precision are unknown. Conceptually, higher WM precision can be achieved by distinguishing mental representations of similar information, which is akin to the process of pattern separation (12). This process has been traditionally ascribed to circuitry of the medial temporal lobe (MTL), for the purposes of serving long-term episodic memory (13, 14). Indeed, the MTL has been considered irrelevant for WM (15), and until recently little neural evidence has directly linked the MTL with WM especially for non-spatial item information (16–18). However, behavioral estimates of WM and long-term memory precision are closely correlated (19). We therefore hypothesize that WM precision also relies upon the MTL. This hypothesis predicts that the MTL should be sensitive to task demands on WM precision, should retain precise item-level WM content, and should causally support WM precision.

To test these predictions, we asked different cohorts of participants to perform a WM recall task (2, 3, 20), as we captured neuroimaging or intracranial EEG (iEEG) data and as we measured behavioral changes in WM precision during direct electrical stimulation of the MTL or following its surgical removal. In this task, participants try to remember items randomly drawn from a continuous circular feature space (color or orientation) and after a short delay recall one of the items as precisely as possible (*Fig. 1A & 1F*). We estimate WM precision as the inverse of the standard deviation (*SD*) of recall errors (3) after factoring out failed recall responses uniformly distributed across the feature space (*Fig. 1B*). Behaviorally, we found that WM precision was closely related to mnemonic discrimination of similar items in a long-term memory task established to infer MTL pattern separation functions (21; *Fig. S1*). The current study therefore aims to provide converging neural evidence to further support the three core predictions of the MTL hypothesis for WM precision.

We first examined how the MTL responds to different levels of precision load in the WM recall task (*Fig. 1C*), while participants were undergoing high-resolution fMRI of the temporal lobe (*Fig. 1D*; Experiment 1,  $n = 18$ ). Under a high-precision load, participants studied and recalled colors randomly sampled from a color wheel of 180 colors (3). Under medium- and low-precision loads, participants studied and recalled colors sampled from 15 and 6 color wedges evenly distributed in the color space, respectively (22). Participants' likelihoods of remembering the study colors were similar across precision loads (*Fig. S2*), yet as the color space becomes finer, the task demand on remembering the exact color hues increases (22). Consistent with the previous finding that the hippocampal DG/CA3 distinguishes similar long-term memory contents (13, 14, 23), we found that DG/CA3 activity monotonically increased with WM precision loads ( $\beta = 0.33, p = 0.015$ ; *Fig. 1E*). This association was absent in other MTL regions (*Fig. S3*). This finding suggests that MTL circuitry that has been previously associated with long-term memory pattern separation is also sensitive to task demands on WM precision.

We next tested the prediction that MTL activity during WM retention reflects item-related WM information as participants performed a separate task established to decode visual WM content from neural signals (24–26). Briefly, participants sequentially viewed two oriented

gratings randomly sampled from 9 evenly-spaced angles in a 180-degree orientation space (*Fig. 1F & S4*; Experiment 2,  $n = 16$ ). We cued participants to retain and later reproduce one of the oriented gratings (24). Using an inverted encoding modeling (IEM) procedure (*Fig. S5*), we replicated previous findings that item-related information is retained in distributed cortical regions during WM retention (24, 25; *Fig. S6*). Of primary interest, we found that the amount of item-level information for the cued item was significantly greater than chance in two anatomically defined MTL regions during WM retention, namely the anterior lateral entorhinal cortex (aLEC;  $t(15) = 4.41, p < .001$ ) and the hippocampal DG/CA3 ( $t(15) = 4.73, p < .001$ ; *Fig. 1G & S7*). This effect was specific to the cued item, as item-level information of the uncued item was indistinguishable from chance ( $t$ 's < 1) and was significantly less than that for the cued item (aLEC:  $t(15) = 2.75, p = 0.015$ ; DG/CA3:  $t(15) = 3.83, p = 0.0016$ ). We replicated these findings using representational similarity analysis (RSA; *Fig. 1H*), which involves fewer analytical assumptions (27). We found that stimulus similarity, inversely related to the absolute angular distance between orientations, was significantly correlated with neural similarity across trials in both the aLEC and the DC/CA3, as compared with shuffled orientations (aLEC:  $t(15) = 4.29, p < .001$ ; DG/CA3:  $t(15) = 3.65, p = 0.0024$ ) and the uncued item (aLEC:  $t(15) = 2.66, p = 0.018$ ; DG/CA3:  $t(15) = 3.65, p = 0.0024$ ). Furthermore, RSA and IEM estimates were highly correlated across individuals (*Fig. S8*). Together, these converging findings indicate that delay-period MTL activity retains precise item-level WM content.

To determine whether the MTL also retains item-level WM content for other stimulus features, we directly recorded iEEG signals from the entorhinal cortex and the hippocampus as participants performed a modified color recall task (*Fig. 2A, 2B, & S9*; Experiment 3,  $n = 13$ ). On each trial, participants tried to remember a single color indicated by a cue over a short retention interval. We applied RSA to 70-150Hz iEEG activity (*Fig. 2C*), given its relevance to single-unit spikes and fMRI signals (28). In the MTL, we found that these high-frequency signals were significantly associated with the cued item as compared with shuffled colors ( $p_{\text{corrected}} < .05$  during 600-1,040 ms after stimulus onset; cluster mean relative to the uncued item,  $t(12) = 2.39, p = 0.034$ ; *Fig. 2D & S10*). In a subset of participants with occipitotemporal electrode coverage ( $n = 6$ ), we found that occipitotemporal signals were also significantly correlated with the cued item but at an earlier time ( $p_{\text{corrected}} < .05$  during 240-600 ms after stimulus onset; cluster mean relative to the uncued item,  $t(5) = 2.90, p = 0.034$ ; *Fig. 2D & S10*). In principle, neural correlates with the cued item while stimuli were presented could reflect both perceptual and WM processes, but their manifestations during the delay period are unlikely driven by perceptual encoding (24–26). If MTL's association with the cued item is due to perceptual processes, item-related variance in MTL signals should be greater in an earlier (0-500 ms) versus a later (500-1,000 ms) time window following stimulus onset (*Fig. 2D*). However, we found that MTL signals were more correlated with the cued item in the late versus the early time window ( $t(12) = 2.70, p = 0.019$ ), whereas the opposite was observed in occipitotemporal signals ( $t(5) = 4.35, p = 0.007$ ; *Fig. 2E*). For participants who had electrodes in both regions, there was a significant region by time interaction ( $F(1,5) = 7.39, p = 0.042$ ; *Fig. S11*). These results indicate that item-related information in the MTL reflects WM retention and is unlikely to be driven by perceptual encoding.

Finally, we examined the causal role of the MTL in WM precision using two complementary approaches. First, in a subset of participants, we electrically stimulated the MTL

5 during the delay period in a random half of the trials while participants performed the WM color recall task (Experiment 4,  $n = 4$ ). We applied charge-balanced biphasic rectangular pulses following the offset of the study items to minimize any impact on perceptual encoding (Fig. 3A). We found that MTL stimulation substantially increased recall variability (hence reducing WM precision) at the group level (difference in SD between *on* and *off*: 4.23 [95% HDI: 0.06, 8.24],  $BF_{10} = 15.67$ ; Fig. 3B), based on Bayesian hierarchical modeling (29), and at the participant level, based on individual best-fit parameters (Fig. S12). Stimulation, however, did not have a significant impact on the probability of recall success,  $P_m$ , which is inversely related to participants' failed recall responses uniformly distributed in the color space (Fig. 1B; difference in  $P_m$  between *on* and *off*: -0.06 [-0.14, 0.04],  $BF_{10} = 0.29$ ). The stimulation-induced increase in recall variability remained robust even when we directly compared the absolute recall errors (Fig. S12) and other models of WM recall performance (Fig. S13).

10

15 Second, we examined WM precision in a group of participants who performed the color WM recall task before and after they received a surgical resection for treatment of epilepsy (Experiment 5,  $n = 14$ ). Half of these participants had a resection of MTL structures (MTL group; Fig. 3C), while the other half either had a resection of other brain regions (e.g., temporal pole or the insula) or had no surgical resection at all (non-MTL group; see Table S4). We found that participants' WM precision markedly decreased following removal of the MTL (difference in SD for *post* vs. *pre*: 5.38 [1.42, 8.89],  $BF_{10} = 60.58$ ; Fig. 3D), with no significant change in  $P_m$  (difference for *post* vs. *pre*: -0.05 [-0.12, 0.02],  $BF_{10} = 0.42$ ). These results also manifest in individual best-fit parameters across MTL cases ( $t(6) = 3.66, p = 0.011$ ;  $P_m$ :  $t < 1$ ; Fig. S14). In contrast, we did not observe a significant effect in either measure for the non-MTL group ( $BF_{10} < 1, t's < 1$ ; Fig. S14). The effect of surgical removal on WM precision was significantly greater in the MTL relative to non-MTL group (interaction effect:  $BF_{10} = 81.21$ ;  $F(1,12) = 9.00, p = 0.011$ ).  
20 These results are unlikely to be driven by surgical effects on perceptual/motor functions as the participants' performance in a control task remains high and comparable before and after surgery ( $t's < 1$ ; Fig. S15). These data demonstrate that MTL perturbations reliably compromise WM precision without affecting the likelihood of encoding an item into WM, which is related to WM capacity (3).  
25

30 Together, our data provide converging evidence from multiple modalities to support the three core predictions of the MTL hypothesis for WM precision. The MTL is sensitive to task demands on WM precision, retains item-level WM content, and plays a causal role in WM precision. These results extend the large literature on frontoparietal contributions to WM capacity (9–11) by identifying an MTL mechanism for WM precision that is similar to that underlying the fidelity of long-term memory (13, 14, 23). Our findings therefore suggest that the MTL may contribute to mnemonic precision for both WM and long-term memory (19) and provide a better understanding for comprised WM and long-term memory precision often seen in aging (7, 8).  
35

## References and Notes:

1. A. D. Baddeley, *Annu. Rev. Psychol.* **63**, 1–29 (2012).
2. P. M. Bays, M. Husain, *Science* **321**, 851–854 (2008).
3. W. Zhang, S. J. Luck, *Nature* **453**, 233–235 (2008).
5. 4. R. van den Berg, H. Shin, W.-C. Chou, R. George, W. J. Ma, *Proc. Natl. Acad. Sci. U. S. A.* **109**, 8780–8785 (2012).
6. N. Cowan, *Behav. Brain Sci.* **24**, 87–185 (2001).
7. S. J. Luck, E. K. Vogel, *Nature* **390**, 279–281 (1997).
10. S. M. Korkki, F. R. Richter, P. Jeyarathnarajah, J. S. Simons, *Psychol. Aging* **35**, 124–142 (2020).
8. W. Xie, A. Berry, C. Lustig, P. Deldin, W. Zhang, *J. Int. Neuropsychol. Soc.* **25**, 583–594 (2019).
9. E. K. Vogel, M. G. Machizawa, *Nature* **428**, 748–751 (2004).
10. J. J. Todd, R. Marois, *Nature* **428**, 751–754 (2004).
15. T. J. Buschman, M. Siegel, J. E. Roy, E. K. Miller, *Proc. Natl. Acad. Sci. U. S. A.* **108**, 11252–11255 (2011).
12. D. Marr, *Philos. Trans. R. Soc. London B Biol. Sci.* **262**, 23–81 (1971).
13. A. Bakker, C. B. Kirwan, M. Miller, C. E. L. Stark, *Science* **319**, 1640–1642 (2008).
14. M. A. Yassa, C. E. L. Stark, *Trends Neurosci.* **34**, 515–525 (2011).
20. W. B. Scoville, B. Milner, *J. Neurol. Neurosurg. Psychiatry* **20**, 11–21 (1957).
16. J. Kamiński *et al.*, *Nat. Neurosci.* **20**, 590–601 (2017).
17. A. Jeneson, L. R. Squire, *Learn. Mem.* **19**, 15–25 (2012).
18. D. E. Hannula, D. Tranel, N. J. Cohen, *J. Neurosci.* **26**, 8352–8359 (2006).
19. W. Xie, H.-B. Park, K. A. Zaghloul, W. Zhang, *Psychol. Sci.* **31**, 345–348 (2020).
25. P. Wilken, W. J. Ma, *J. Vis.* **4**, 11 (2005).
21. S. M. Stark, M. A. Yassa, J. W. Lacy, C. E. L. Stark, *Neuropsychologia* **51**, 2442–2449 (2013).
22. W. Zhang, S. J. Luck, *Psychol. Sci.* **22**, 1434–1441 (2011).
23. Z. M. Reagh, M. A. Yassa, *Proc. Natl. Acad. Sci. United States Am.* **111**, E4264–E4273 (2014).
30. 24. E. F. Ester, T. C. Sprague, J. T. Serences, *Neuron* **87**, 893–905 (2015).
25. K. C. Bettencourt, Y. Xu, *Nat. Neurosci.* **19**, 150–157 (2015).
26. S. A. Harrison, F. Tong, *Nature* **458**, 632–635 (2009).
27. N. Kriegeskorte, M. Mur, P. Bandettini, *Front. Syst. Neurosci.* **2**, 1–28 (2008).
35. 28. S. Haufe *et al.*, *Neuroimage* **179**, 79–91 (2018).
29. K. O. Hardman, E. Vergauwe, T. J. Ricker, *J. Exp. Psychol. Hum. Percept. Perform.* **43**, 30–54 (2017).

**Acknowledgments:** We thank Stephanie Leal, Nicholas J. Tustison, Zachariah Reagh, Jason Langley, Julio Chapeton, Vishnu Sreekumar, and Dave Youssef for technical support and constructive comments. We are indebted to all the participants who selflessly volunteered their time to take part in this study.

5

**Funding:** This work was supported by Intramural Research Program of the National Institute of Neurological Disorders and Stroke (ZIA-NS003144, PI: K. Z.) and Extramural Research programmes of the National Institute of Mental Health (1R01MH117132, PI: W. Z.). W.X. was funded by the National Institute of Neurological Disorders and Stroke Competitive Postdoctoral Fellowship Award.

10

**Author contributions:** **Weizhen Xie**: Conceptualization, Methodology, Software, Data curation, Writing - Original Draft, Visualization, Project administration, Funding acquisition. **Marcus Cappiello, John Jr. Wittig, Srijan Bhasin, Christopher Zawora, Michael A. Yassa, Edward Ester, Sara K. Inati**: Methodology, Software, Data curation, Writing - Review & Editing. **Kareem A. Zaghloul, Weiwei Zhang**: equally contributed to Supervision, Conceptualization, Methodology, Writing - Review & Editing, Funding acquisition.

15

**Competing interests:** Authors declare no competing interests.

20

**Data and materials availability:** All data and materials are available upon request.

#### **Supplementary Materials:**

Materials and Methods

25

Figures S1-S15

Tables S1-S4

References (1-80)

30

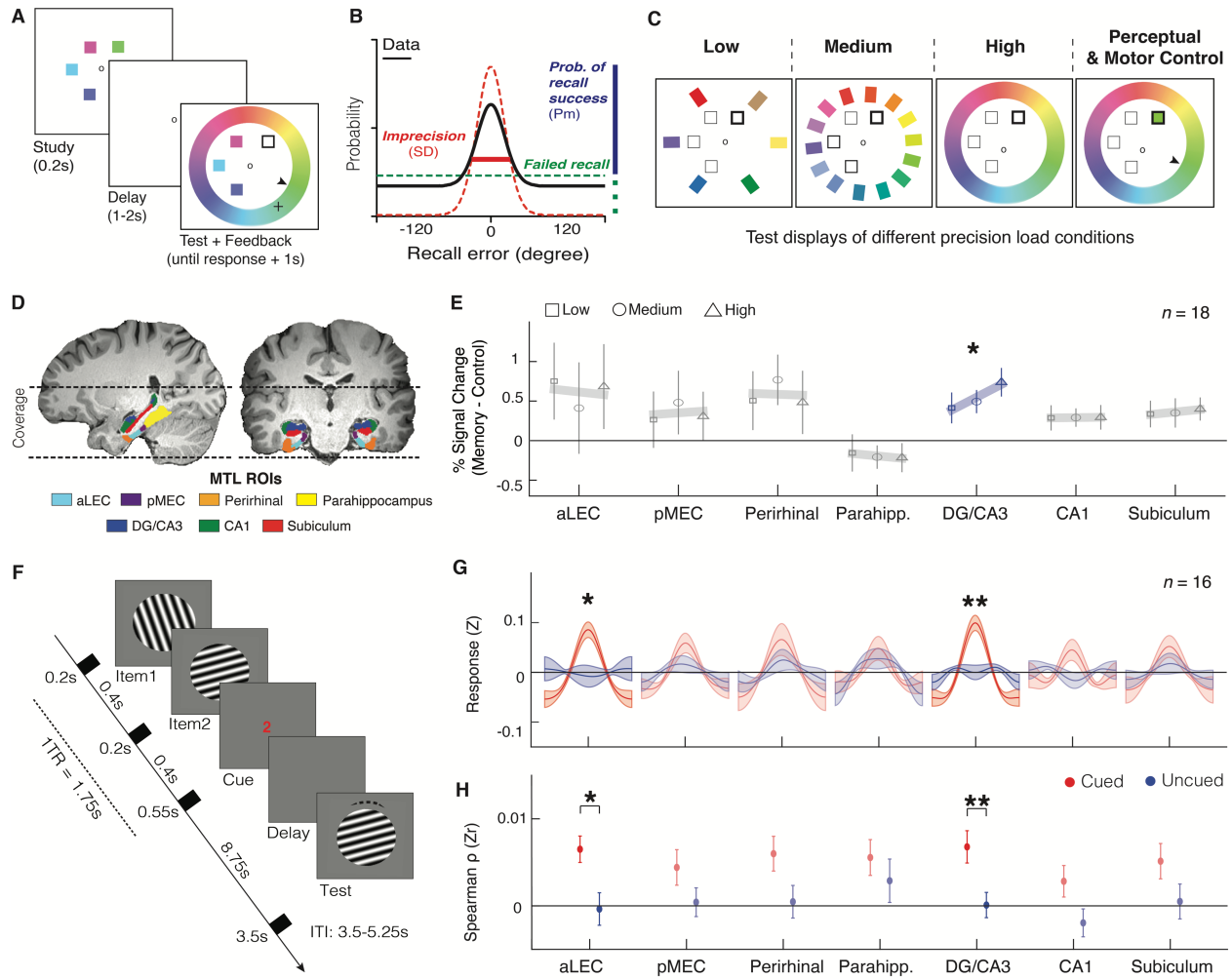


**Fig. 1. The MTL is sensitive to task demands on WM precision and retains item-related WM content.** (A) Example of the WM recall task. (B) Participants' recall errors (black) are modeled as a mixture of retained WM information with some variability (imprecision, red) and failed memory responses uniformly distributed in a feature space (green). (C) The numbers of study-and-test colors were parametrically varied to manipulate precision load in Experiment 1. (D) High-resolution fMRI coverage over the temporal lobe with MTL regions parcellated based on previous research (23). (E) fMRI signals (memory vs. control condition) monotonically increase with WM precision load in DG/CA3. (F) Participants performed a retro-cue WM orientation recall task in Experiment 2. We used inverted encoding modeling (G) and representational similarity analysis (H) to assess item-related WM content from delay-period MTL activity. Shaded areas and error bars represent standard error. \* $p < .05$ ; \*\* $p < .01$  (cued relative to uncued in G and H). aLEC = anterior lateral entorhinal cortex; pLEC = anterior medial entorhinal cortex.

5

10

15

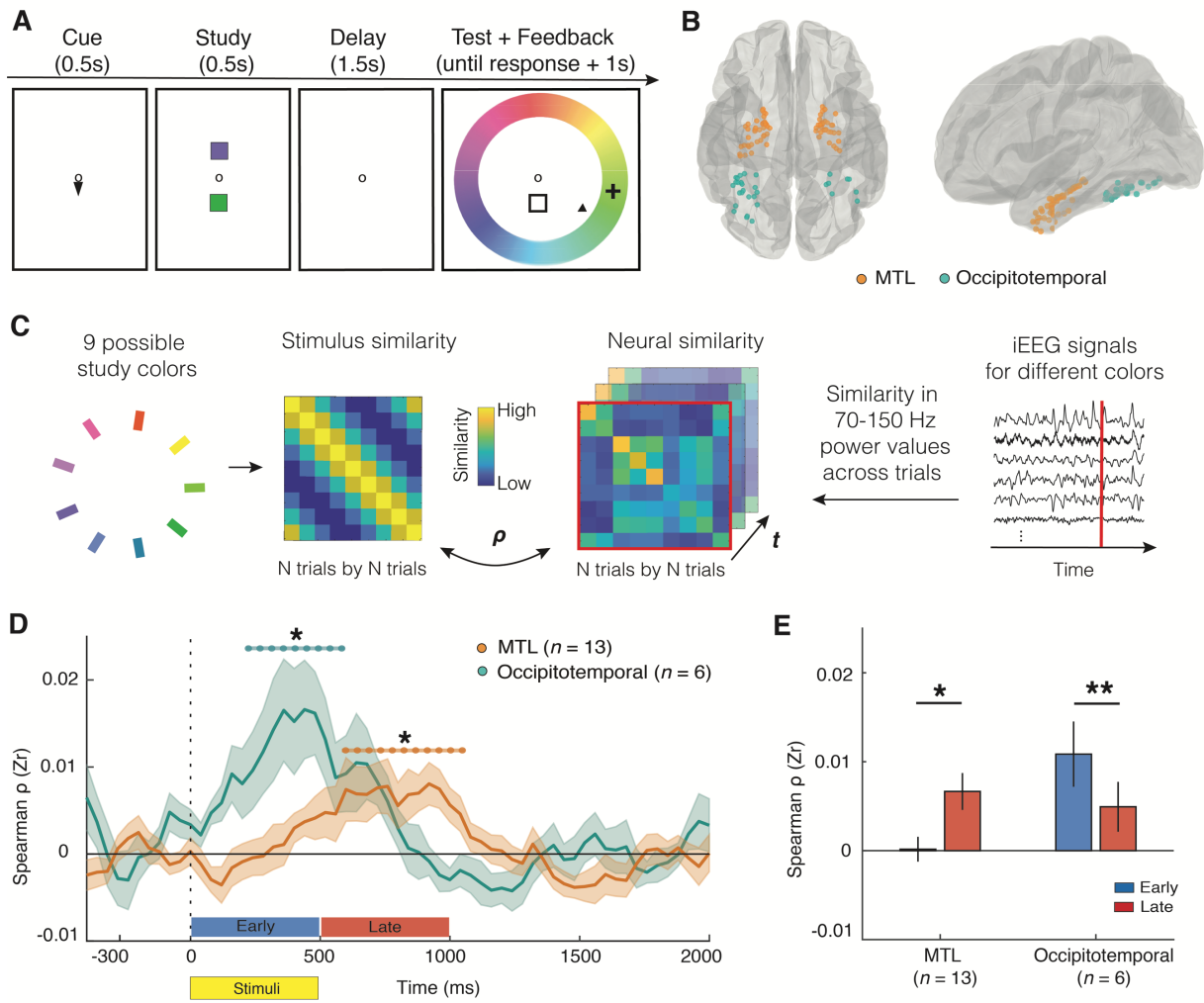


**Fig. 2. Delay-period MTL activity contains item-related WM variance revealed by iEEG recordings.** (A) Participants performed a pre-cue WM color recall task in Experiment 3. (B) Electrode distribution across subjects in the MTL and the occipitotemporal cortex. (C) For each time point, trial-by-trial stimulus similarity pattern is correlated (Spearman rank-order) with trial-by-trial neural similarity pattern to capture item-related variance of the cued item in the neural data. (D) MTL signals are significantly associated with the cued item during WM delay period, whereas occipitotemporal association with the cued item mostly manifests while the item was on the screen (also see Fig. S10). (E) MTL signals are more correlated with the cued item during a late (500–1,000 ms) versus an early (0–500 ms) time window following stimulus onset, whereas occipitotemporal signals show the opposite pattern (see Fig. S11 for results from subjects with electrodes in both regions). Shaded areas and error bars represent standard error. \* $p < 0.05$  (after cluster-based correction in D), \*\* $p < 0.01$ .

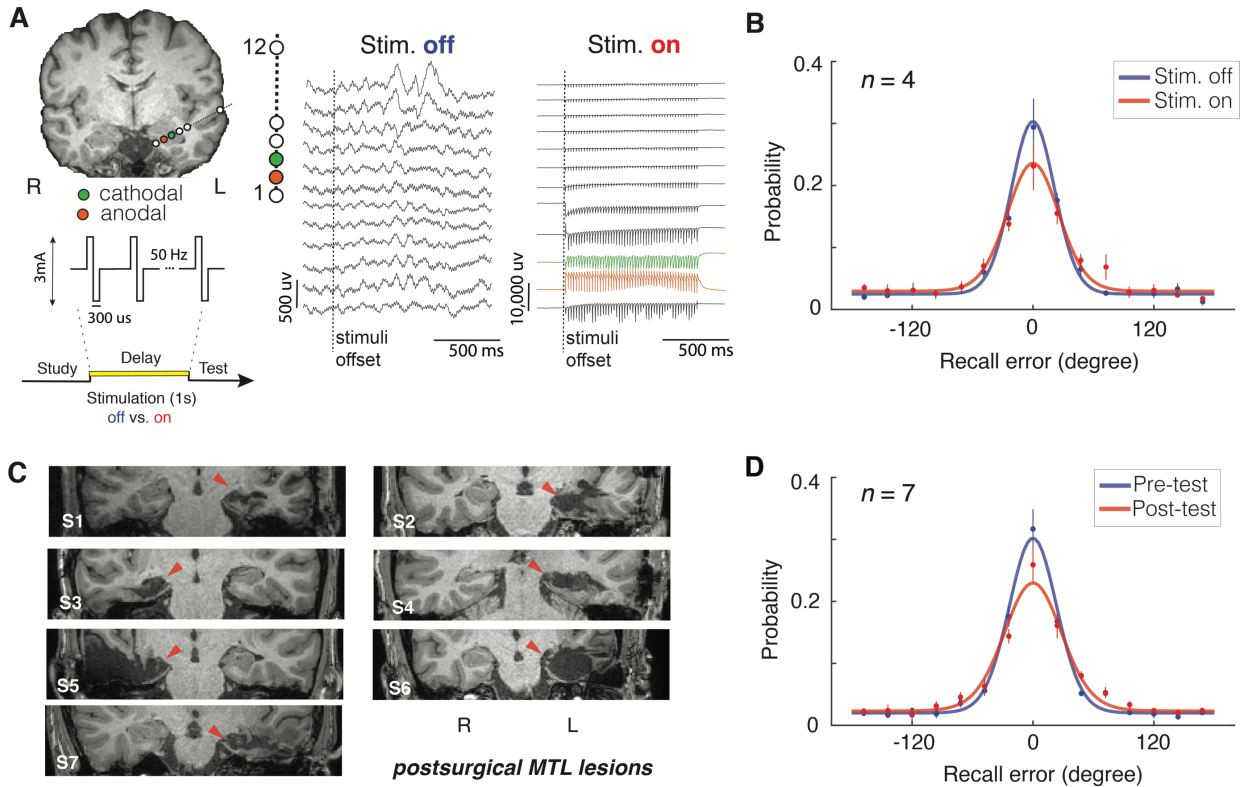


**Fig. 3. Perturbing the MTL with direct electrical stimulation or surgical lesion**

**substantially reduced WM precision.** (A) Charge-balanced biphasic rectangular pulses were randomly delivered across trials via a pair of adjacent hippocampal electrodes following offset of study items throughout the 1-s delay period, as participants were performing the WM color recall task in Experiment 4 (*Left*). This stimulation substantially affected ongoing MTL activity (*Right*), and markedly reduced participants' WM precision (B), increasing their recall variability. (C) Participants' with lesions in the MTL (see *Table S4*). (D) MTL lesions also markedly reduced participants' WM precision in Experiment 5. For (B) and (D), error bars are standard errors, and the fitted lines are average posterior patterns from the Bayesian hierarchical modeling analysis.

5

10

15

## Supplementary Materials for

### **The Medial Temporal Lobe Supports Visual Working Memory Precision**

Weizhen Xie<sup>1,2\*</sup>, Marcus Cappiello<sup>2</sup>, John H. Wittig Jr.<sup>1</sup>, Srijan Bhasin<sup>1</sup>, Christopher Zawora<sup>1</sup>, Michael A. Yassa<sup>3</sup>, Edward Ester<sup>4</sup>, Sara K. Inati<sup>5</sup>, Kareem A. Zaghloul<sup>1\*†</sup>, Weiwei Zhang<sup>2\*†</sup>

\*Correspondence to: Weizhen Xie ([weizhen.xie@nih.gov](mailto:weizhen.xie@nih.gov), ORCID: 0000-0003-4655-6496),  
Kareem A. Zaghloul ([kareem.zaghloul@nih.gov](mailto:kareem.zaghloul@nih.gov), ORCID: 0000-0001-8575-3578), and Weiwei  
Zhang ([weiwei.zhang@ucr.edu](mailto:weiwei.zhang@ucr.edu), ORCID: 0000-0002-0431-5355).

†Senior authors contributed equally to this work and are listed in alphabetical order.

#### **This PDF file includes:**

Materials and Methods  
Figs. S1 to S14  
Tables S1 to S4  
References (1-80)

## Materials and Methods

### Participants

A total of 115 participants ( $23.72 \pm 0.73$  years old [Mean  $\pm$  s.e.m], 64 females) were recruited for different experiments of this study (see *Tables S1* and *S2* for details). All participants reported normal color vision and normal or corrected-to-normal visual acuity. The sample size is consistent with previous research using similar methods in respective experiments. In brief, we screened and recruited 34 healthy young adults for fMRI experiments ( $n = 18$  in Experiment 1 at the University of California, Irvine and  $n = 16$  in Experiment 2 at the University of California, Riverside; see *Table S1*). All of these healthy volunteers were right-handed and reported no history of neurological or psychiatric disorders or prior psychostimulant use. Additionally, we recruited 60 college students at the University of California, Riverside for Experiment S1. We compensated all the healthy volunteers with either \$20/hour or course credits for their participation, and the compensation was not conditioned on their task performance.

We also recruited 21 participants (Wechsler Intelligence Quotient [IQ]:  $88.87 \pm 3.63$ , all  $> 70$ ; see *Table S2*) with drug-resistant epilepsy for experiments performed at the Clinical Center of the National Institutes of Health (NIH; Bethesda, MD). These participants required surgically implanted subdural and/or sEEG (stereo-electroencephalogram) recordings as part of their evaluation for epilepsy surgery. During intracranial EEG (iEEG) monitoring, participants completed a color WM recall task (Experiment 3,  $n = 13$ ). As permitted by clinical safety and electrode location, a subset of participants performed another color WM recall task as we stimulated the hippocampus through a pair of adjacent sEEG contacts (Experiment 4,  $n = 4$ ). In addition, participants performed the color WM recall task and a perceptual and motor control task before (1-2 days) and after (1-3 months) surgical resection of the brain region responsible for their seizures (Experiment 5,  $n = 14$ ).

All participants or their guardians provided written, informed consent following the procedures approved by the Institutional Review Board of each local research site. Except where otherwise noted, all computational analyses were performed using MATLAB (MathWorks; Natick, MA).

### Behavioral Paradigms

Across different experiments of this study, participants performed a WM recall task using a delayed-estimation paradigm (2, 3, 20). In this paradigm, participants first try to remember a set of briefly presented study items that are randomly sampled from a continuous circular feature space. In different versions of the task, participants remember either a color or the orientation of a grating. After a short delay, participants then try to recall and reproduce one of the study items as precisely as possible in the corresponding feature space (Fig. 1A and 1F). We measured memory performance as the angular difference, henceforth referred to as recall error, between the studied and reported feature values on each trial (3). Except where otherwise specified, we presented stimuli on a 60 Hz LCD monitor with a gray background at a viewing distance of ~57 cm.

WM color recall task with precision load manipulation (Experiment 1). Participants performed this task inside of an MRI scanner. On each trial, we presented 4 perceptually different color squares ( $\sim 2.5^\circ \times 2.5^\circ$  of visual angle) on the screen for 200 ms after an initial 2000 ms blank screen with a fixation circle. The locations of these colors were randomly selected from a set of 8 equally spaced locations on an invisible circle ( $\sim 5.5^\circ$  of visual angle in radius). Participants were asked to remember these colors over an 1,800-ms delay interval. During the test phase of each trial, we presented four placeholders at the original locations of the study colors along with a surrounding circular color spectrum ( $\sim 8^\circ$  of visual angle in radius). We rotated the circular color spectrum presented during test by a random angle on every trial to minimize spatial biases. Participants tried to reproduce one of the colors at one of the locations that was randomly chosen and highlighted (Fig. 1A). Participants indicated the remembered color by matching the recalled color onto the circular color spectrum. Specifically, participants pressed one of the two buttons on a response box with the right index or middle finger to move the cursor clockwise and counterclockwise, respectively, until they found the matching color. To confirm their choice, the participants could press a third button using the ring finger. If a response was not confirmed within the response time window (3,750 ms), we treated the last location of the cursor on the color space as the response. Participants' median response time across trials was  $2,979 \pm 165$  ms on average.

We parametrically varied the number of possible study-and-test colors to manipulate WM precision load (22, 30). In the high-precision load condition, the study colors are randomly sampled from 180 colors in the  $360^\circ$  Commission Internationale de l'Eclairage (CIE) Lab color space. These colors have equal luminance and vary mainly in hue and slightly in saturation (3). This set of 180 colors is used throughout the experiments in the present study. In the medium- and low-precision load conditions, the study colors are randomly sampled from a fixed set of 15 and 6 colors, respectively, that are evenly distributed in the circular color space. In the low-precision load condition, the 6 colors are centered around the subjectively reported color categories identified within the set of 180 colors (3) to further reduce the need to encode the precise color hue. In the test phase, we presented the color spectrum consisting of the set of possible colors for the study items (Fig. 1C). After the participant's response, we provided feedback for 500 ms as an arrow pointing at the location of the true test color on the color space. To isolate memory-related from perceptual/motor-related fMRI signals, we also included a perceptual/motor control condition. In this condition, participants viewed visual stimuli similar to those in the memory conditions, but the test color remained at the center of screen with the matching color directly marked on the color spectrum (Fig. 1C). Participants simply tried to move the cursor to the marked color.

We divided the experiment into blocks of trials, with each block corresponding to an experimental condition. Participants completed 2 sequential blocks of each WM condition and 1 block of the perceptual/motor control condition for a total of 7 blocks. Each block consists of 50 trials, yielding 350 total trials per participant. Before each block, we informed each participant which condition they were going to complete. We counter-balanced the order of different conditions across participants using a Latin-square design. Before scanning, participants practiced 50 trials across 2 blocks for each of the 3 WM conditions and 25 trials for the perceptual/motor control condition.

WM orientation recall task (Experiment 2). Participants performed an orientation WM task adapted from previous studies (24, 26) inside an MRI scanner. Briefly, on each trial, we

sequentially presented two sine-wave gratings ( $\sim 4.5^\circ$  of visual angles in radius, contrast at 80%, spatial frequency at  $\sim 1$  cycle per visual degree, randomized phase) at the center of the screen. Each grating appears for 200 ms, with a 400-ms blank screen in between. The two gratings have different orientations randomly drawn from nine predefined orientations (0 to  $160^\circ$  in  $20^\circ$  increments) with a small random angular jitter ( $\pm 1^\circ$  to  $5^\circ$ ). Following the offset of the second grating of each pair by 400 ms, we presented a cue (“1” or “2”, corresponding to the first or second grating, respectively) for 550 ms to indicate which grating orientation the participant should remember and maintain over an 8,750-ms delay period. We instructed participants to remember only the cued grating and to ignore the other. After the delay period, we presented a test grating initially aligned to a random orientation. Participants then pressed the response box buttons to adjust its orientation until it matched the orientation of the cued grating, in the same way as Experiment 1. We asked the participants to make a response within 3,500 ms following the onset of the test grating (averaged median response time across participants:  $2,929 \pm 156$  ms) and we used the orientation of the test grating at the end of this interval as the final response when a response was not confirmed within the response period. After the response, we provided feedback to participants by presenting a line marking the correct orientation, which is followed by an inter-trial interval of 3,500 or 5,250 ms. Participants completed 10 blocks of 18 trials, yielding a total of 180 trials. All experimental factors, namely the cue position and the orientation of presented gratings, are randomly intermixed within each block.

*WM color recall task during iEEG recordings (Experiment 3).* Participants performed a modified color WM task (9) as we captured iEEG recordings from participants with intracranial electrodes. This task is similar to the color WM task used in the high-precision load condition of Experiment 1 (Fig. 2A). However, in this version of the task our goal was to decode the content of a single item in WM. We therefore designed this version of the color WM task to use a prospective cue that instructed the participants to retain just one color in memory. In this task, each trial starts with an arrow cue pointing either to the upper or to the lower visual field for 500 ms. Afterwards, two distinct color squares ( $\sim 2^\circ \times 2^\circ$  of visual angle) aligned along the vertical meridian are presented for 500 ms. The central locations of these color squares deviate from the central fixation by  $\sim 4^\circ$  of visual angle. Both colors are randomly sampled from a fixed set of 9 colors evenly distributed across the 180-color set (3) and are presented with a random offset ( $\pm 0$  to  $10^\circ$ ) in the color space. Participants are instructed to only pay attention to and remember the color indicated by the arrow cue over a 1500-ms delay period. During the test phase, participants recall the color originally presented in the cued location, which is randomly chosen across trials, by clicking the corresponding color on a wheel with the 180 colors as precisely as possible using a computer mouse. At the end of a trial, a feedback arrow pointing to the true color appears for 1000 ms, followed by a 1,000- to 2,000-ms random inter-trial interval. In the current sample, each participant performed 10 to 18 blocks of 18 trials each (see Table S3 for details). All experimental factors, including study color identities and cue locations, are randomly intermixed within each block.

*WM color recall task during in-vivo electrical stimulation (Experiment 4).* Participants performed a version of the color WM task similar to the high-precision load condition in Experiment 1 and to previous research in clinical populations (31) while we delivered direct electrical stimulation to probe the causal role of the MTL in WM precision. In this version of the task, on each trial we presented 3 colors randomly sampled from the 180 colors for 200 ms. After a short retention interval of 1000 ms, participants recalled one of the missing colors highlighted

by an empty square placeholder via a mouse click on the test color wheel. All but one color were presented on the screen to minimize mis-binding in participants' responses (32). On half of the trials, we delivered a weak electrical current during the 1000-ms retention interval immediately following the offset of the study array. The details of electrical stimulation are specified in a later section. On the other half of the trials, we delivered no stimulation. After an initial 12 trials of practice, each participant completed 7 to 10 blocks of 36 trials (see *Table S3*). All experimental factors, including study color identities, color locations, and stimulation conditions, are randomly intermixed within each block.

*WM color recall task in patients with brain lesions (Experiment 5).* Participants performed a WM color recall task with a perceptual/motor control condition 1-2 days before their first electrode implant surgery and 1-3 months after their resection or electrode removal surgery. All experimental parameters for the task are identical to those in Experiment 4. In addition to the WM recall task, we also included 30 trials of a perceptual and motor control task at the beginning of a testing session. In this control task (31), participants view 3 color squares presented on the screen for 200 ms. Immediately afterwards, they click on the color wheel to report the color highlighted by an outline square while the to-be-reported color remained on the screen. No immediate feedback is given. That is, the true color is not marked on the color wheel after the response. This control condition is included to test whether the participants are able to properly perceive and identify colors before and after their resection surgery (8, 31). After the initial 30 trials of the perceptual/motor control task, participants completed 150 trials of the color WM recall task, divided into 5 blocks of 30 trials each, with all experimental factors intermixed within a block.

*Behavioral measures of mnemonic precision and lure discrimination (Experiment S1).* To assess individual differences in the behavioral estimates of mnemonic precision and pattern separation, we asked participants to first perform an established mnemonic similarity task (21), followed by two color-recall tasks capturing WM and long-term memory precision (3, 33). We counterbalanced the order of the two recall tasks across participants. The WM recall task (*Fig. S1A*) used here is identical to that in Experiments 4 and 5 with one exception: we increased the memory set size to 5 and present the study items for 400 ms in order to better measure WM capacity in college-student participants with a typical WM capacity of 2 to 3 colors (3, 5).

In the long-term memory recall task (*Fig. S1B*), 120 unique objects are randomly chosen from a stimulus set of 540 everyday objects (33, 34). In the study phase, the objects are sequentially presented in random order (2,000 ms presentation time with a 1000-ms inter-stimulus-interval). The color of each object is randomly sampled from the 180 colors. Participants are explicitly instructed to remember the colors of the presented objects. In the subsequent test phase, the objects from the study phase are sequentially presented in grey scale and random order. Participants are asked to reproduce the color of each object as precisely as possible with the object staying on the screen until response. Specifically, the participants continuously adjust the object's color, by moving the computer mouse along a circle that represents an invisible color wheel of the 180 colors (34), until it best matches the remembered color. The mouse's location is initially set at the center of the grey-scale object whose color updates in real time with the mouse movement (33–35). Participants completed 2 study-and-test blocks with 60 objects per block.

In the mnemonic similarity task (*Fig. S1C*), each trial starts with an incidental study phase during which 128 images of everyday objects are sequentially presented (2000 ms presentation time each, with a 1000-ms inter-stimulus interval) in a random order (21). Participants report whether the image contains an indoor or outdoor object by pressing the V and N keys on a standard keyboard, respectively. In the test phase, 192 test objects are sequentially presented in random order. One-third of these objects are exact repetitions of those presented in the study phase (old); another one-third are lures that are visually similar, but not identical, to those seen during the study (similar); and the remaining one-third are novel items not previously seen (new). Participants press different keys to indicate whether the test object is “old” (V), “similar” (B), or “new” (N). We assessed each participant’s ability to separate similar memory patterns using the lure discrimination index,  $P(\text{“similar”} \mid \text{Lure}) - P(\text{“similar”} \mid \text{New})$ , which corrects for the general response bias to respond “similar” even to novel items in the test phase (12). As a behavioral measure of the pattern separation function, the lure discrimination index can reliably correlate with MTL activity (22, 23), be perturbed by transcranial direct current stimulation over the anterior temporal lobes (47), and shows a decline with MTL lesions (24).

### Behavioral Modeling

We analyzed participants’ recall errors using a mixture model (3, 36). According to this model (*Fig. 1A*), mnemonic precision is inversely defined as the standard deviation (*SD*) of recall errors after factoring out failed memory responses. Failed memory responses manifest as uniformly distributed recall errors, especially when study items are randomly sampled from a circular feature space (36, 37). The uniformity of the recall error distribution is hence inversely related to probability of recall success ( $P_m = 1 - \text{Probability of uniform distribution}$ ), which is proportional to the number of the remembered items (22, 36). This model, in general, provides a good fit to participants’ recall performance (across participants:  $R^2 > 98\%$ ) (36, 38). We also considered alternative models for our data that differ from one another mostly in the interpretation of the tails of the recall error distribution (2, 4, 39, 40). Because our analyses primarily focused on the central peak of the recall error distribution instead of its tails, our results on recall variability across experimental conditions remain compatible with results based on other models. It should be noted that the number of recall options is reduced in the medium- and low- precision load conditions in Experiment 1. This limits our ability to estimate the precision of retained WM content in these conditions (22). However, even in this case, it is still appropriate to estimate the amount of failed memory responses using a uniform distribution in the feature space (3, 22). Therefore, we partitioned recall errors into 12 bins and fit these binned data using the Simplex method (41) to estimate  $P_m$  in Experiment 1. We also compared the probability of large-error responses (absolute error  $\geq 90^\circ$ ) across conditions using a Chi-squared test (*Fig. S2*). In either case, participants’ tendency for random responses was statistically non-distinguishable across precision load conditions in Experiment 1, in line with the previous observations (22).

### MRI Data Acquisition and Pre-processing (Experiments 1 and 2)

We acquired neuroimaging data using 32-channel sensitivity encoding (SENSE) coils in

3.0 Tesla scanners at the University of California, Irvine (Philips Achieva, Experiment 1) and the University of California, Riverside (Siemens Prisma, Experiment 2). The scanning sequences were optimized for different experiments and scanners. For Experiment 1, we acquired a high-resolution 3D magnetization-prepared rapid gradient echo (MP-RAGE) structural scan (0.65 mm isotropic voxels) at the beginning of each session. Functional MRI scans consisted of a T2\*-weighted echo-planar imaging (EPI) sequence using blood-oxygenation-level-dependent (BOLD) contrast: TR = 2500 ms, TE = 26 ms, flip angle = 70 degrees, 37 slices, 160 dynamics per run,  $1.8 \times 1.8 \text{ mm}^2$  in-plane resolution, 1.8 mm slice thickness with a 0.2 mm gap, FOV = 180 mm  $\times$  74 mm  $\times$  180 mm. This sequence, with a focus on the MTL regions (Fig. 1D), has been previously validated to capture MTL sensitivity to stimulus similarity in long-term memory (42, 43). We acquired a total of 7 functional runs for each participant: 6 for the memory conditions (2 for each memory condition) and 1 for the perceptual/motor control condition. Each functional run lasted 6 minutes and 40 seconds excluding the 4 initial dummy scans acquired to ensure T1 signal stabilization. For Experiment 2, we optimized the scanning sequence for high-resolution functional MRI with whole-brain coverage. Following a MP-RAGE structural scan (0.8 mm isotropic voxels), we acquired 10 functional runs with the following settings: TR = 1750 ms, TE = 32 ms, flip angle = 74°, 69 slices, 189 dynamics per run,  $1.5 \times 1.5 \text{ mm}^2$  in-plane resolution with 2 mm slice thickness, FOV read = 222 mm, FOV phase = 86.5%. Each functional run lasted 5 minutes and 30.75 seconds. In the end of the experiment, we acquired two additional scans with opposite phases to correct for EPI distortions (44).

We preprocessed neuroimaging data using the Analysis of Functional NeuroImages (AFNI) software (45). Briefly, functional data were de-spiked (*3dDespike*), slice timing corrected (*3dtshift*), reverse-blip registered (*blip* in Experiment 2), aligned to structural scan (*align\_epi\_anat.py*), motion corrected (*3dvolreg*), and masked to exclude voxels outside the brain (*3dautomask*). Data from Experiment 1 were blurred to 2 mm isotropic (*3dmerge*) with a Gaussian FWHM kernel to increase the signal-to-noise ratio (42, 43), and then modeled based on the canonical hemodynamic function with a temporal derivative (SPMG2) time-locked to the onset of the WM study items (*3dREMLfit*). We controlled for head motions (movement exceeded about 3° of rotation or 3 mm of translation in any direction relative to the prior time point) and the voxels that had more than 10% outliers. In Experiment 2, to avoid introducing artificial autocorrelations in later analyses (see the section below), functional data were not smoothed. For the same reason, we extract the raw BOLD signals from the middle 3 TRs of the 5-TR retention interval for later analyses without fitting the data to the hemodynamic model (24).

We defined participant-specific MTL ROIs (hippocampal DG/CA3, CA1, and subiculum, anterior and posterior entorhinal cortex, perirhinal cortex, and parahippocampus, see Fig. 1D) based on prior research (42, 43) by aligning an in-house template to each participant's brain (46, 47). For functional analysis, we combined DG and CA3 subfields as a single label given the uncertainty in separating signals from these two subfields in fMRI data (42). We combined data from bilateral MTL ROIs in later analyses.

### Inverted Encoding Modeling (IEM, Experiment 2)

To decode item-level information from the raw BOLD signals (24), we first constructed a linear encoding model to represent orientation-selective responses in multi-voxels of activity

from a given brain region (48). We assumed that the response of each voxel is a linear summation of 9 idealized information channels (*Fig. S5*), estimated by a set of half-wave rectified sinusoids centered at different orientations based on the tuning profile of orientation sensitive neural populations (49, 50). Hence, we formalized the observed raw BOLD signals  $\mathbf{B}$  ( $m$  voxels  $\times$   $n$  trials) as a weighted summation of channel responses  $\mathbf{C}$  ( $k$  channels  $\times$   $n$  trials), based on the weight matrix,  $\mathbf{W}$  ( $m$  voxels  $\times$   $k$  channels), plus residual noise ( $N$ ),

$$\mathbf{B} = \mathbf{WC} + \mathbf{N}$$

Given  $\mathbf{B}_1$  and  $\mathbf{C}_1$  from a set of training data, the weight matrix can be calculated as,

$$\mathbf{W} = \mathbf{B}_1 \mathbf{C}_1^T (\mathbf{C}_1 \mathbf{C}_1^T)^{-1}$$

The training weight matrix  $\mathbf{W}$  is used to calculate a set of optimal orientation filters (51, 52),  $\mathbf{V}$ , to capture the underlying channel responses while accounting for correlated variability between voxels (i.e., the noise covariance), as follows,

$$V_i = \frac{\sum_i^{-1} W_i}{W_i^T \sum_i^{-1} W_i}$$

where  $\Sigma_i^{-1}$  is the regularized noise covariance matrix for channel  $i$  (1 to 9), estimated as,

$$\Sigma_i^{-1} = \frac{1}{n_1 - 1} \varepsilon_i \varepsilon_i^T$$

$$\varepsilon_i = \mathbf{B}_1 - \mathbf{W}_i \mathbf{C}_{1,i}$$

Here,  $n_1$  is the number of training trials, and  $\varepsilon_i$  is a matrix residual based on the training set  $\mathbf{B}_1$  and is obtained by regularization-based shrinkage using an analytically determined shrinkage parameter (52). Next, for the independent hold-out test dataset  $\mathbf{B}_2$ , trial-by-trial channel responses  $\mathbf{C}_2$  are calculated as follows,

$$\mathbf{C}_2 = \mathbf{V}^T \mathbf{B}_2$$

We used a leave-one-out cross-validation routine to obtain reliable estimate channel responses for all trials. For each participant, in every iteration we treated all but one block as  $\mathbf{B}_1$  and the remaining block as  $\mathbf{B}_2$  for the estimation of  $\mathbf{C}_2$ . This analysis yielded estimated channel responses  $\mathbf{C}_2$  for each trial, which were interpolated to 180°, circularly shifted to a common center (0°, by convention). We reconstructed these normalized channel responses separately using orientation labels of the cued item, the uncued item, and shuffled orientations. We then quantified the amount of item-related information ( $R$ ) by converting the average channel response ( $z$ ) to polar form given  $\psi$  as the vector of angles at which the channels peak ( $z = Ce^{2i\psi}$ ). We then projected them onto a vector with angle 0,

$$R = |\bar{z}| \cos(\bar{\psi})$$

With whole-brain coverage, we performed a searchlight procedure in combination with the IEM analysis (24). First, we aligned individual structural and functional data to a common space (MNI, Montreal Neurological Institute) using the Advanced Normalization Tools (53, 54).

Second, we defined a spherical “neighborhood” (radius 8.0 mm) centered on voxels in a cortical mask containing only gray matter voxels. We discarded neighborhoods with fewer than 100 voxels (24). Last, after we estimated item-related information ( $R$ ) about the to-be-remember item based on the IEM analysis outlined above, we combined participants’ data using *3dMEMA* with a one-sample  $t$ -test on  $R$  at each voxel against the chance level (mean  $R = 0$ ). We then applied a cluster-based correction procedure to identify significant voxels across participants (one-tailed,  $p < 0.05$ , FWER corrected based on *3dClustSim*).

### Representational Similarity Analysis (RSA) for MTL Patterns (Experiment 2)

To evaluate the delay-period activity with fewer analytical assumptions, we conducted RSA (27), complementary to the IEM analysis. First, we calculated the neural similarity pattern across trials. We compared the delay-period signals  $B$  across  $n$  voxels from the middle 3 TRs between every pair of trials. As a result, we obtained a trial-by-trial similarity matrix in which the similarity between voxel response vectors  $B_i$  and  $B_j$  was calculated as,

$$S(I_i, Q_j) = \frac{B_i * B_j}{||B_i|| ||B_j||}$$

We next calculated the stimulus similarity pattern across trials using 180 minus the absolute angular distance between the orientation labels of every two trials. Finally, we correlated (Spearman rank-order) the neural similarity pattern and stimulus similarity pattern across trials to estimate the item-related variance in the neural data. We assumed that similar items should be represented more closely in the neural data as compared with dissimilar items. We found that this RSA approach captures item-related variance revealed by the IEM (*Fig. S8*).

We limited this analysis to the trials with recall error within 3 standard deviations of the recall error distribution based on behavioral model fits for each participant, as the cued item is likely retained in WM on these trials. With this criterion, less than 3% of the trials were excluded (out of 180 trials per participant; *Fig. S4*). We performed this analysis using trial labels separately based on the cued item and to the uncued item. To obtain an empirical null-effect correlation within each participant, we shuffled each participant’s cued orientation labels across 5000 times and took the average of these values. We Z-transformed these Spearman rank-order correlations before performing the group-level comparison.

### Intracranial EEG Recordings, Pre-processing, and Analysis (Experiment 3)

We recorded iEEG signals from both subdural and depth electrodes (PMT Corporation, Chanhassen, MN) sampled at 1000 Hz using a Nihon Kohden (Tokyo, Japan) or a Blackrock Microsystems (Salt Lake City, UT) iEEG data acquisition system. Subdural contacts are arranged in grid or strip configuration with an inter-contact spacing of 5 or 10 mm. Depth electrodes have 8 to 16 contacts spaced 2 to 5 mm apart and a diameter of 0.8 mm. We localized electrode contacts by co-registering postoperative CT and preoperative MRI images using established methods (55). We projected resulting contact locations from each individual participant to a normalized MNI cortical surface for visualization. In this study, we focused on

electrode contacts in the MTL, primarily in the hippocampus or entorhinal cortex, and the occipitotemporal cortex (*Fig. 2B*). These regions were defined based on cortical parcellation labels using *FreeSurfer*. On average, we included  $11.69 \pm 1.24$  electrodes per participant for analysis after preprocessing steps below (*Table S3*).

First, for each recording session, we rejected noisy electrode contacts with an average amplitude or variance greater than 3 standard deviations of the mean estimates from all electrode contacts. We removed slow fluctuations from the signals using a local detrending procedure and removed line noise at 60 Hz and 120 Hz. The remaining iEEG traces were then bipolar referenced based on the participant-specific electrode montage. Henceforth, we refer to these bipolar referenced signals as electrodes. Second, we rejected additional electrodes and trials that showed excessive signal kurtosis or variance during epochs of individual trials (56). In brief, we calculated the variance of the iEEG trace for each electrode during a 5000-ms epoch time-locked to the onset of WM study items (-2000 to 3000 ms). This task related epoch included a 1000-ms buffer data at the beginning and at the end. We computed the channel-by-trial matrix of variance measures, from which we identified each trial or channel data with outliers, defined by data values greater than the third quartile plus 2.3 times of the inter-quartile range (56). Together, these two steps removed most iEEG signals potentially contaminated by interictal activity, movement-induced artifacts, or transient electrical perturbations by external sources.

We next quantified spectral power in each temporal epoch (encoding and retrieval) by convolving the cleaned iEEG signals with complex-valued Morlet wavelets (wave number 6) at different frequencies (40 logarithmically spaced values from 3 to 150 Hz). We squared and log-transformed the extracted values to generate a continuous measure of instantaneous power at each frequency. Next, we z-scored the power values separately for each frequency and for each session using the mean and standard deviation of all respective values from that session (57). Finally, we removed the 1000-ms buffered data at the beginning and at the end of each epoch and extracted z-scored power traces for each frequency and each electrode during task-related periods for later analyses (56).

We then analyzed the iEEG data using the RSA approach to minimize analytical assumptions. The RSA procedure used for the iEEG data is similar to that outlined for fMRI analysis in Experiment 2 with the following exceptions. First, to obtain a vector of high-frequency signals in a brain region across trials, we extracted and concatenated the z-scored power of 8 log-spaced broadband (70 to 150 Hz) iEEG power values of each electrode. We binned these continuous feature vectors over time into 400-ms epochs spaced every 40 ms (90% overlap), starting from -400 ms prior to cue onset to the test array onset in the WM recall task. We next calculated the neural (cosine) similarity pattern between every pair of trials at each time bin based on the feature vectors in these trials. We then calculated the Spearman rank-order correlation between the high-frequency iEEG neural similarity pattern and the stimulus similarity pattern of the stimuli between trials that is based on the absolute angular distance between every two colors in the circular color space. To maximize the inclusion of trials in which participants retained the cued item, we limited this analysis to the trials with recall errors within 3 standard deviations of the recall error distribution. This criterion led to less than 18% of total trials being excluded from the analyses, as participants' probability of recall success was about 83% on average (*Fig. S4*). In the end, we included  $226.08 \pm 13.68$  trials per participant for this analysis after iEEG artifact removal and exclusion of trials with large recall errors (see *Table S3*).

### In-vivo Electrical Stimulation (Experiment 4)

As the availability of electrode locations was strictly determined by clinical needs, we prioritized participants who had hippocampal electrodes based on electrode localization as previously described (55). Before the stimulation session, a neurologist performed a standard clinical functional mapping procedure to identify candidate hippocampal sites and to confirm the safety of stimulation at those sites. In this procedure, electrical stimulation (charge-balanced biphasic rectangular pulses, pulse width = 300  $\mu$ s, at 50 Hz, *Fig. 3A*) was delivered at a pair of adjacent hippocampal sites at an initial peak-to-peak amplitude of 0.5 mA for 1 s while the neurologist monitored for after-discharges. This procedure was repeated, incrementing the amplitude in steps of 0.5 mA, up to a maximum of 3-mA peak-to-peak amplitude. Once a pair of hippocampal electrode sites was confirmed to evoke no after-discharges, we proceeded with stimulation using 3 mA peak-to-peak amplitude for the rest of the experiment.

We used Blackrock Microsystems (Salt Lake City, UT) software to program and control the delivery of the stimulation, which was triggered by the offset of the study items. We randomly delivered the stimulation during the 1,000-ms WM retention period on half of the trials within each experiment block. This procedure minimized the direct impact of electrical stimulation on perceptual processing of the study items. In addition, the stimulation was double-blind such that during the experiment the neurologist, the experimenter, and the participant could not predict whether electrical stimulation would be delivered on a given trial. Throughout the experiment, the neurologist monitored participants' responses to the electrical stimulation. All participants reported that they were not aware of the stimulation, and the neurologist observed no clear after-discharges as a result of the electrical stimulation in the experiment.

### Statistical Analyses

We used complementary approaches to evaluate the statistical evidence in the data. For neural data in Experiment 1, 2, and 3, we compared participants' averaged neural measures (e.g., % change in BOLD signal, averaged IEM or RSA evidence within a time window) based on conventional statistical procedures, including t-tests, contrast analysis (58, 59), repeated-measures analysis of variance (ANOVA), and mixed-effect linear modeling. For IEM and RSA analyses, to estimate an empirical chance level, we repeated the analysis (IEM or RSA) by shuffling the item labels across trials over 5000 iterations (with replacement) and computing the average. Except where otherwise specified, all  $p$ -values reported are two-tailed against these empirical null values. We found that the  $p$  values from conventional statistical procedures could be reproduced using non-parametric tests or resampling procedures (60), suggesting that analytical assumptions have a minimal effect on the conclusions of our findings. When appropriate, we corrected for multiple comparisons by using Bonferroni correction or cluster-based procedure (56) with an alpha level set as 0.05.

For the analyses of the behavioral data in Experiments 4 and 5, we obtained converging evidence using different methods. In Experiment 4, to evaluate participants' recall performance across different stimulation conditions, we first fitted the data using a Bayesian hierarchical modeling approach as previously described (29, 32, 61, 62). This approach estimates the participant-level best-fit parameters while simultaneously incorporating both between-participant

and within-participant uncertainty (29, 63). We compared the amount of evidence in the posterior distributions across stimulation conditions estimated from 10,000 Markov Chain Monte Carlo iterations (after 5000 burn-in iterations) against uninformative priors (location 0 and a scale value of 2 for  $Pm$  and 5 for  $SD$ ). We gauged the likelihood of the data under the alternative hypothesis relative to the null hypothesis, namely the Bayes Factor ( $BF_{10}$ ), using the Savage–Dickey method (64, 65). We implemented this procedure via the *CatContModel* R package (29), verified by in-house scripts using *Stan* (32, 66, 67). We reported both the 95% high density interval (HDI) of the posterior distribution for the difference of a given parameter between conditions along with its  $BF_{10}$ . A  $BF_{10}$  greater than 3 indicates substantial evidence in favor of the data under the alternative hypothesis relative to the null hypothesis (61, 68). Note, as the priors were uninformative, they had a minimal impact on the group-level posteriors (29, 69).

We then supplemented these Bayesian results with individual best-fit MLE parameters by combining data from each participant meta-analytically (70, 71), given the limited sample size in Experiment 4. First, we extracted participants' best-fit MLE parameters from the mixture model. Next, we created a null distribution separately for each participant by randomly shuffling the condition labels over 5000 times (60). We then compared the observed conditional difference in the data relative to this null distribution to obtain an empirical  $p$  value each participant. We converted these  $p$  values to  $r$ -equivalent effect size estimates, and combined the Fisher's Zr transformed effect size across participants in a mixed-effect meta-analysis (71). To complement these model-based analyses, we also analyzed the data in a model-free manner by directly comparing the absolute recall errors across stimulation conditions. These additional analyses yielded consistent findings as those from the hierarchical Bayesian modeling (see Fig. S12).

Finally, for Experiment 5, we obtained converging evidence from Bayesian hierarchical modeling (29, 32) and individual best-fit MLE parameters, as well as absolute recall errors, in a mixed-effect repeated-measures ANOVA. In this ANOVA, we used testing time points (i.e., before and after neurosurgery) and lesion groups (MTL-related vs. non-MTL-related lesions) as within-group and between-group factors, respectively. The interaction effect of this ANOVA tells us whether the effect sizes of WM measures due to surgical lesions are significantly different from one another across different lesion groups. We also examined participants' performance in the perceptual/motor control task, based on the absolute response errors, using a similar mixed-effect repeated-measures ANOVA.

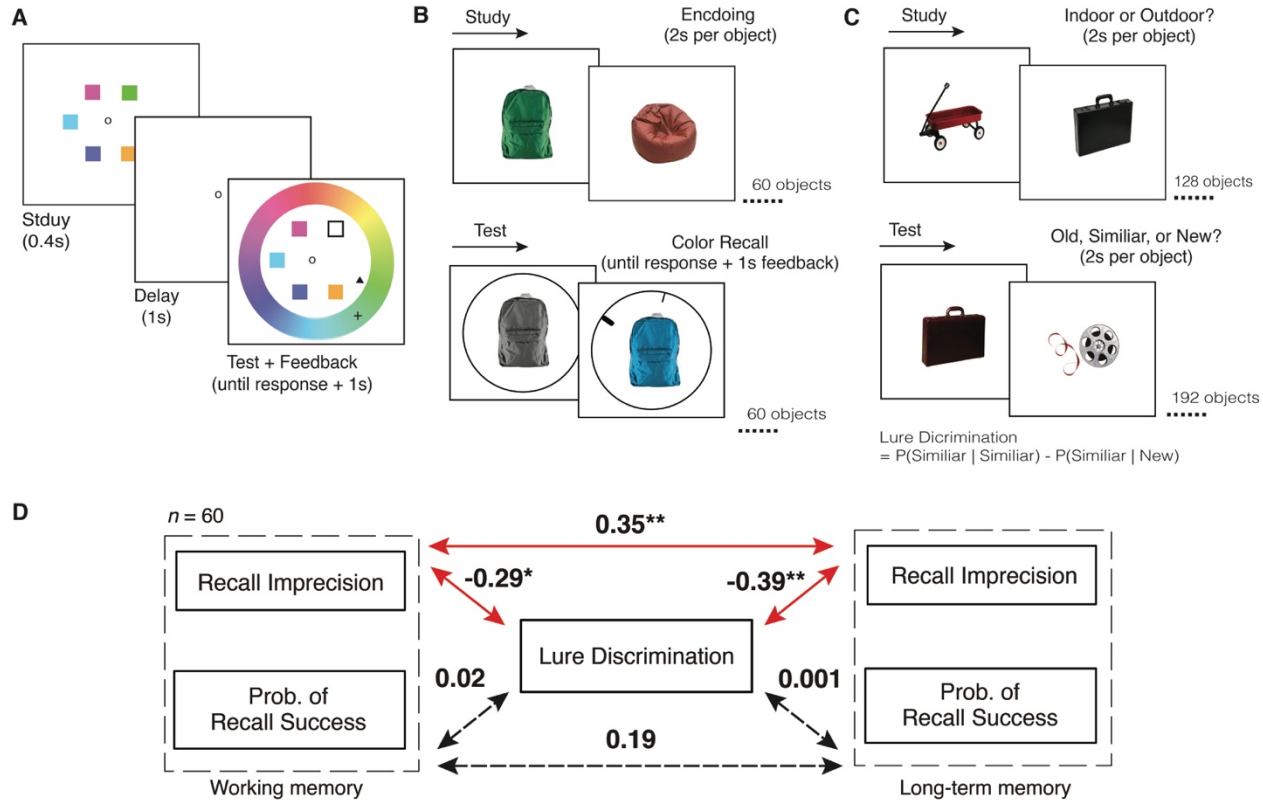


**Fig. S1.** The behavioral estimate of MTL pattern separation function is closely associated with individual differences in mnemonic precision across WM and long-term memory. In Experiment S1, participants' mnemonic precision in WM and long-term memory was estimated from recall errors in the WM (A) and the long-term (B) color recall tasks (3, 33), respectively. We estimated participants' pattern separation function as the ability to discriminate lure items from previously encountered items (21) in the mnemonic similarity task (21), administered at the beginning of the experimental session (C). (D) We found that individuals with higher lure discrimination showed better mnemonic precision, hence smaller recall variability, in both the WM ( $r = -0.29, p = 0.026$ ) and long-term ( $r = -0.39, p = 0.002$ ) color recall tasks ( $n = 60$ ). However, lure discrimination was not significantly correlated with the probability of recall success in either WM or long-term memory ( $p > .50$ ). Critically, the correlation between lure discrimination and mnemonic precision across WM and long-term memory (Fisher's  $Zr = -0.35$ ) was significantly stronger than the correlation between lure discrimination and the probability of recall success across WM and long-term memory (Fisher's  $Zr$  mean = 0.01,  $p = .008$ , resampled over 5000 times). These findings suggest that there is a significant amount of variance shared across the behavioral measures of the qualitative, but not the quantitative, aspect of WM and long-term memory (19). Significant correlation values between variables of interest are marked as red solid lines, whereas nonsignificant values are marked as black dashed lines in (D).

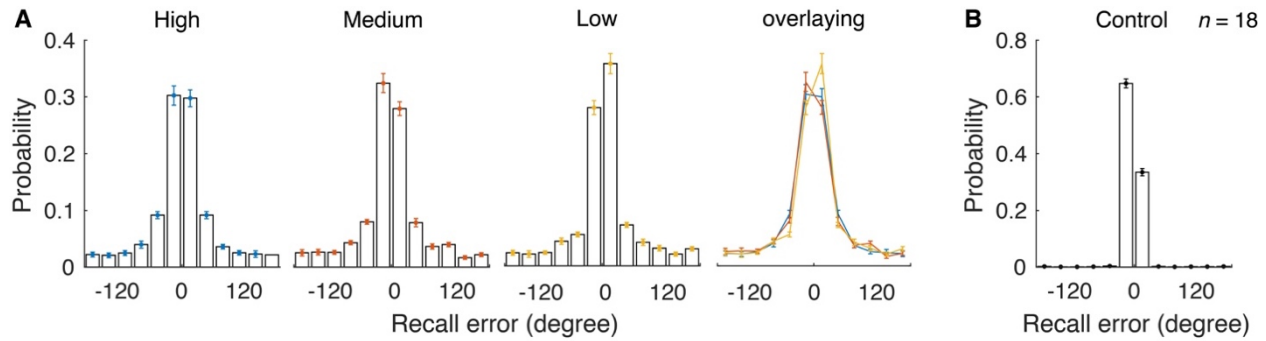


**Fig. S2. Behavioral recall error distributions in Experiment 1.** **(A)** Participants' recall performance in the WM conditions was highly consistent with previous observations (22). That is, they retained a comparable amount of information across different precision load conditions, as indicated by comparable tails of the recall error distributions across conditions. We tested this by partitioning the recall error distribution into 12 bins, determined by the low-precision load condition with 6 possible color spokes, using model-free and model-based statistics. First, without fitting the recall error distribution to a model, we directly compared the counts of trials with an absolute recall error greater than 90-degree in the binned recall error distributions across memory conditions. These large error trials are highly likely to result from unsuccessful recall (3). A Chi-squared test across bin counts of these larger error trials suggested that the amount of uniformness in the tails of the recall error distributions was statistically indistinguishable across memory conditions ( $\chi^2 < 1$ ). Second, using a model-based approach, we fitted the binned recall data to the mixture model using the *Simplex* method (41). Repeated-measures ANOVA showed no significant difference in  $P_m$  (on average  $70\% \pm 14\%$ ) across the WM conditions ( $F(2, 34) = 0.45$ ,  $p = .64$ ,  $\eta^2_p = .026$ ). **(B)** Participants' performance in the perceptual/motor control condition were at ceiling. Error bars represent standard errors.

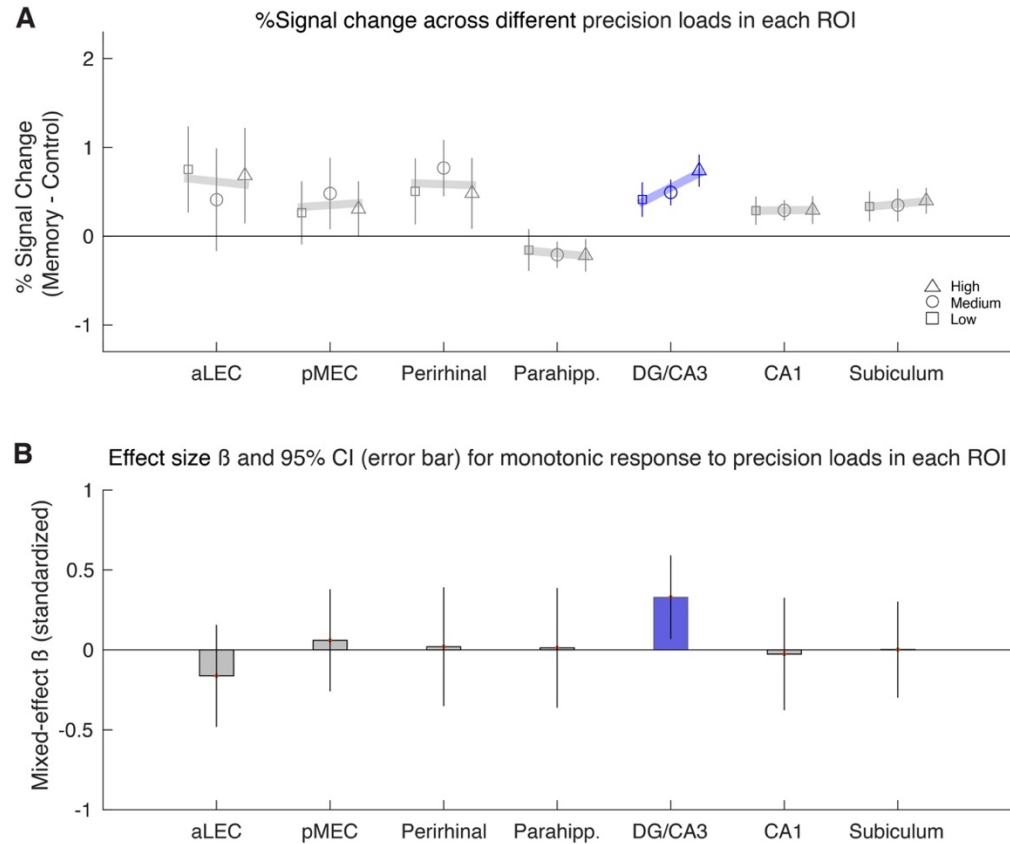


**Fig. S3. MTL sensitivity to WM precision load manifests mostly in the hippocampal DG/CA3 in Experiment 1.** (A) MTL sensitivity to precision load manipulation was restricted to the hippocampal DG/CA3, as the beta value across precision loads (B) was significantly greater in the DG/CA3 than those in other MTL regions based on an *a priori* contrast analysis (59). In this analysis, we predicted that the DG/CA3 should be most sensitive to item-similarity manipulation, as compared with other MTL regions, based on previous research (23). Hence, within each subject, we signed the highest contrast weight (+6) to the beta value of the DG/CA3 and equally small weights (-1) to the beta values of the remaining six MTL regions. If our prediction was not true, the weighted sum of these beta values should be 0 on average across subjects. We found that the weighted sum of these beta values was significantly greater than 0 ( $t(17) = 2.65, p = 0.018$ ), following our prediction. However, this observation did not preclude the possibility that other MTL ROIs also retained WM information. Indeed, based on post-hoc  $t$ -tests, the overall activation level in the memory conditions averaged across precision loads was higher than that in the perceptual/motor control condition (memory – control) in MTL ROIs excluding the para-hippocampus ( $t(17) = 3.06, p = 0.007$ ; the same analysis for the para-hippocampus only:  $t(17) = -1.19, p = 0.25$ ). There was a significant difference in memory-related MTL activation level (memory – control) between other MTL regions as a whole and the parahippocampus ( $t(17) = 3.37, p = 0.004$ ). This observation is in line with recent intracranial recording evidence that the MTL tends to show increase activity (e.g., spike rate) during WM retention in general (16, 72, 73). Error bars represent standard errors. Each data point in (B) represents a value from a single participant. \*\*.  $p < .01$ .

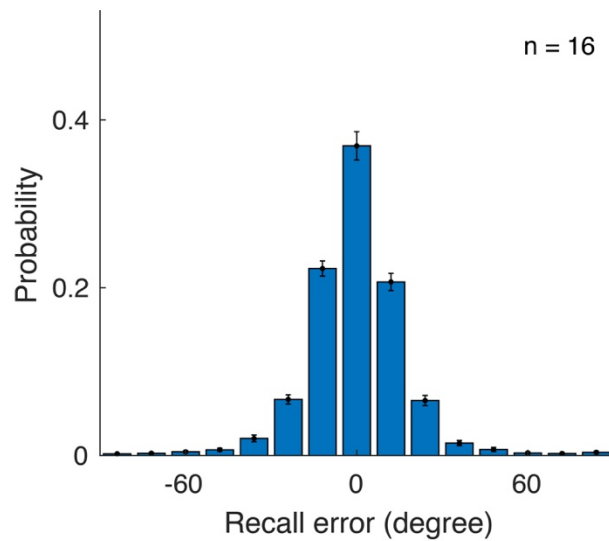


**Fig. S4. Participants' recall performance for the WM orientation recall task in Experiment 2.** Overall, participants' performance in this task was high for both probability of recall success ( $P_m = 0.97 \pm 0.01$ ) and precision ( $SD = 13.29 \pm 0.59$ ), on par with the previous findings in the literature (24). Error bars represent standard errors of mean estimates across participants.

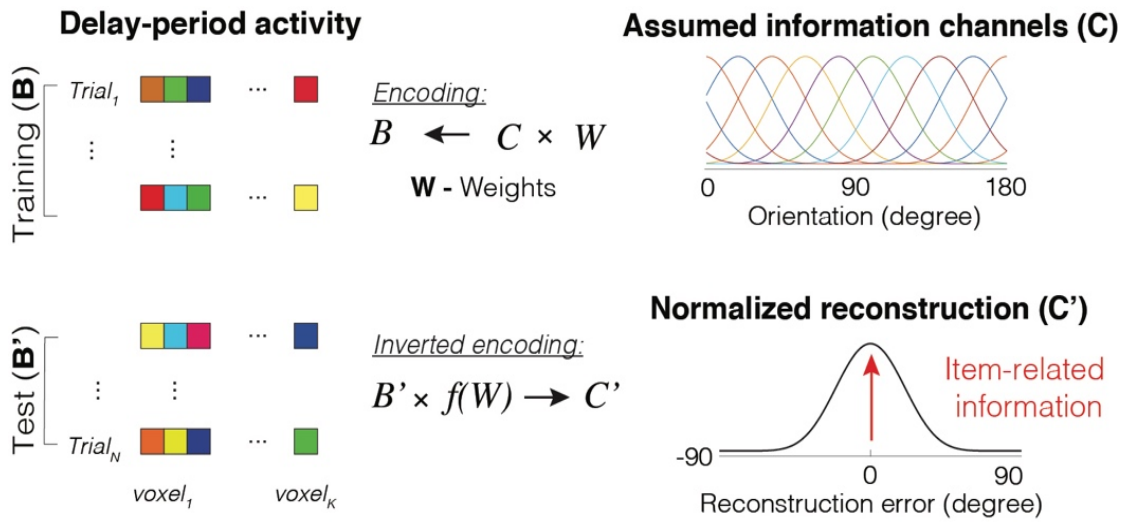


**Fig. S5. Inverted encoding modeling (IEM) procedure.** This procedure assumes that multi-voxel brain activity ( $B$ ) reflects a weighted summation of preferred orientation information channels ( $C$ ) of recorded neural populations (24, 50, 74). The weights ( $W$ ) of these orientation channels can be learned from delay-period activity in a training dataset, and then applied to an independent hold-out test dataset to reconstruct the orientation information channels ( $C'$ ). The resultant vector length of the normalized channel response function can be interpreted as a measure of WM precision, when the probability of recall success is high (75).

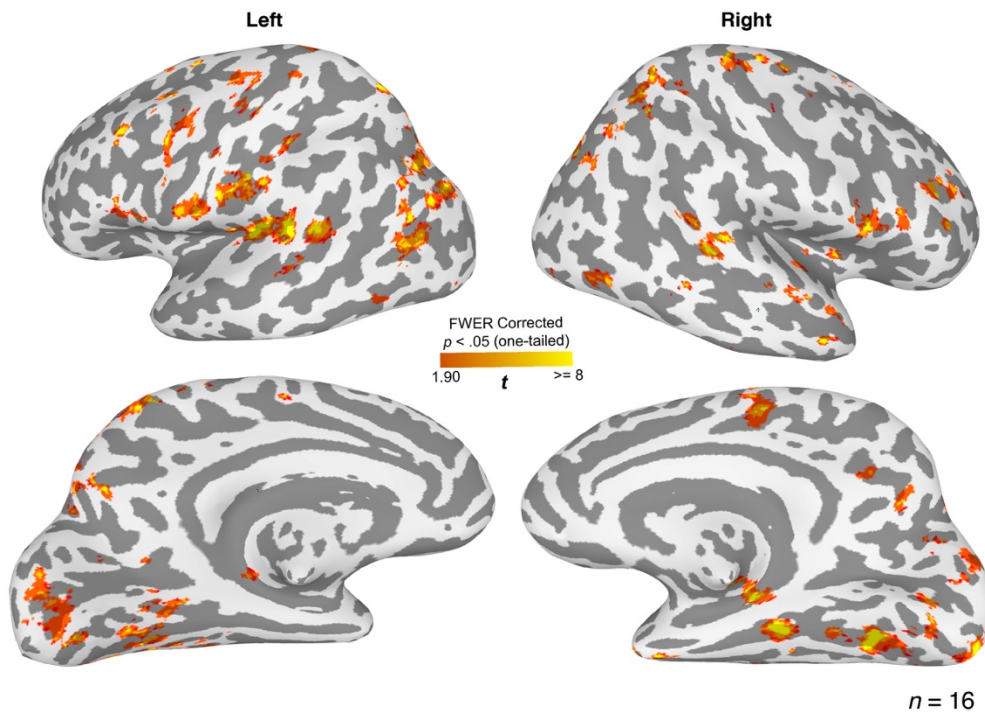


**Fig. S6. Whole-brain searchlight analysis reveals distributed regions retaining information about the cued item during the middle 3TR of the 5-TR delay period in Experiment 2.** A roving searchlight procedure in combination with the IEM analysis was performed to further identify other brain regions containing item-related WM content for the cued item. First, individual structural data were normalized to a high-resolution MNI template (0.8 mm isotropic voxels) using the Advanced Normalization Tools (53). Parameters from these transformations were also used to transform functional data into the template MNI space for later group-level comparisons. Second, in the subsequent searchlight analysis, roving spherical clusters (8 mm radius) centered on each voxel in a cortical mask containing only gray matter voxels for each participant (24) were used to decode item-related information from the weighted average BOLD signals in the middle 3 TRs of the delay period in each trial. Spheres with fewer than 100 voxels were discarded, yielding an average cluster size of 209 voxels (with a maximum size of 257 voxels). Last, group-level results were evaluated by calculating a one-sample t-test at each voxel (*3dMEMA*) to identify regions that robustly contained item-specific information regarding the cued orientation during WM delay period. Group-level *t* values for the resultant vector length of the reconstructed orientation information channels were then projected to a cortical surface in the MNI space. Significance level was set as .05 (one-tailed) after the correction of multiple comparisons (*3dClustSim*). This analysis showed that distributed brain regions retained decodable item-specific information for the cued orientation, which is highly consistent findings in previous studies (24–26).

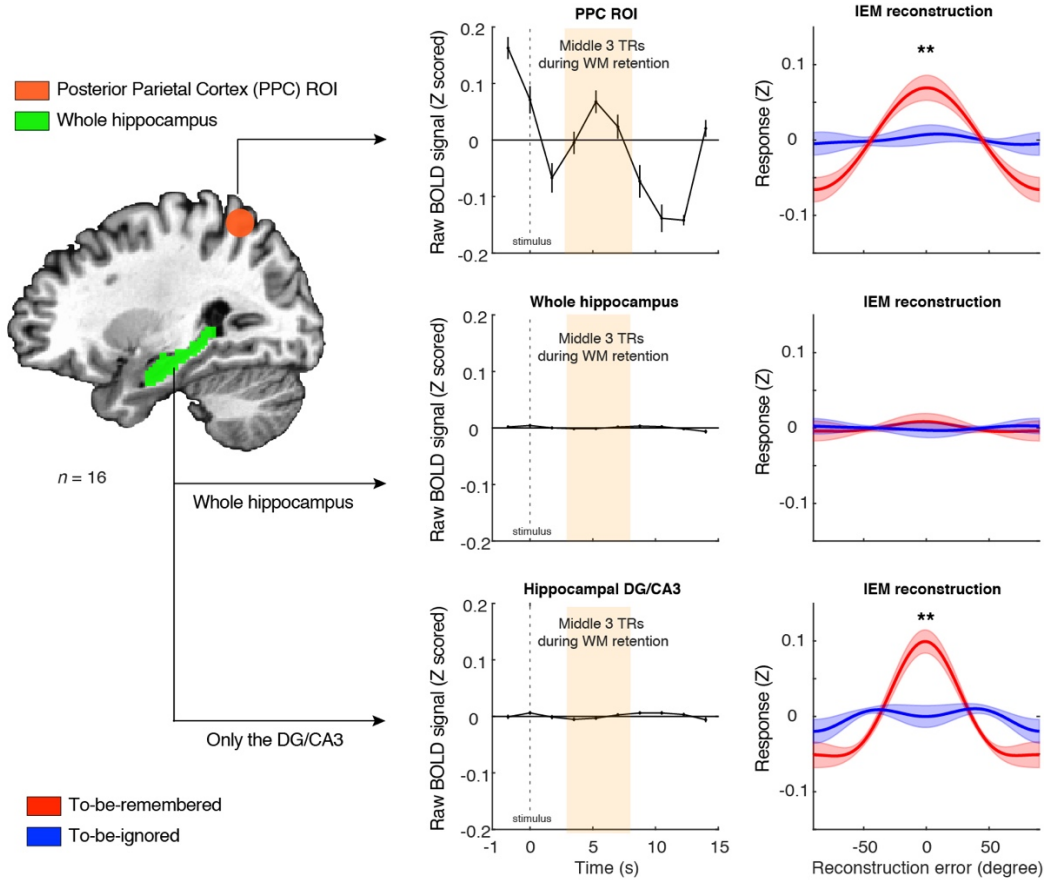


**Fig. S7. IEM analysis based on the whole hippocampus, as compared with the posterior parietal cortex, does not reveal item-related WM content in delay-period activity in Experiment 2.** IEM analysis in selected brain regions (*Left*) revealed several observations that are consistent with the literature, and also add to our understanding of the MTL involvement in WM. First, in the posterior parietal cortex (PPC), we found sustained BOLD activity during the WM delay period as well as a robust reconstruction of item-related information. These observations are in line with previous findings (9, 10, 24, 25). For visualization, we plotted the raw BOLD trace averaged across participants (*Top, middle*) from two 8-mm spheres centered at the local peak of the bilateral parietal cluster based on the searchlight analysis in *Fig. S6* (MNI coordinate: left,  $x = -16$ ,  $y = -64$ ,  $z = 58$ ; Right,  $x = 30$ ,  $y = -56$ ,  $z = 58$ ), and the corresponding IEM reconstruction results from this bilateral ROI (*Top, right*). Second, in the hippocampus as a whole, we also did not find sustained BOLD activity or the IEM reconstruction of the item-related WM information during the delay interval as in prior research (24). However, when we focused on the hippocampal DG/CA3 subfield based on high-resolution fMRI data, we found that IEM could reveal item-related WM content, even without significant BOLD modulation for the DG/CA3 during WM retention. This observation is in line with the previous findings from the literature that multi-voxel pattern analysis is sensitive to reveal item-related WM information, even without significant BOLD activity averaged across voxels (24, 25, 76, 77). These observations, therefore, highlight the importance and necessity of high-resolution fMRI in revealing how different MTL subregions may contribute to the short-term retention of precise WM information. \*\* $p < .01$  when comparing the amount of reconstructed information for the cued item relative to the uncued item.

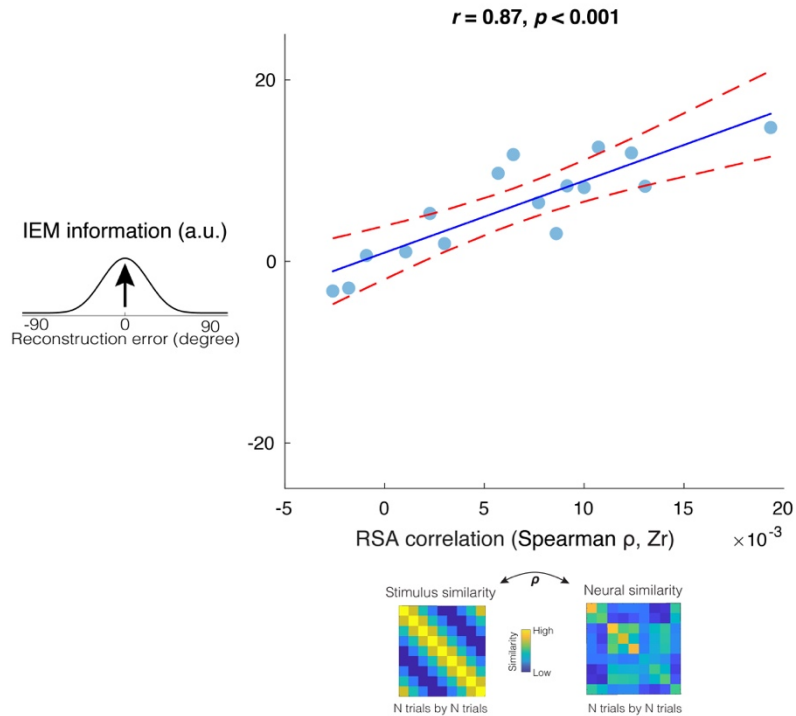


**Fig. S8. Representational similarity analysis (RSA) and inverted encoding modeling (IEM) reveal shared item-related variance in the observed neural data in Experiment 2.** Based on data from an example MTL ROI (aLEC), the association between patterns of task stimuli and neural responses (RSA) was highly correlated with IEM decoding performance across participants ( $r = 0.87, p < .001$ ), even though these two methods have different assumptions and analytical procedures. This observation suggests that item-related WM content in MTL regions can be reliably captured by different analytical procedures, because both procedures capture item-related variance in the neural data. Data on the x-axis are RSA correlation values between trial-by-trial stimulus similarity patterns and observed neural similarity patterns of fMRI BOLD activity in an example MTL ROI (aLEC). Data on the y-axis are the resultant vector length of the normalized reconstructed orientation information channels based on IEM analysis from the same region. Individual points represent the results from the aLEC of an individual participant in Experiment 2. The solid lines are linear fits of the data, and the dashed lines are 95% confidence intervals of the linear fits.

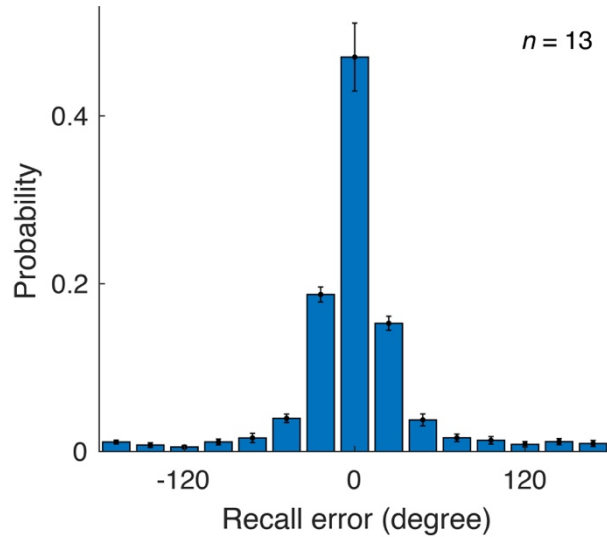


**Fig. S9. Participants' recall performance for the WM color recall task in Experiment 3.**  
Participants' performance in this task was also high and on par with some previous findings (24). Overall, both probability of recall success ( $P_m = 0.83 \pm 0.04$ ) and precision ( $SD = 19.18 \pm 1.48$ ) were high, suggesting that precise item-related information was retained in WM during the experiment. Error bars represent standard errors of mean estimates across participants.

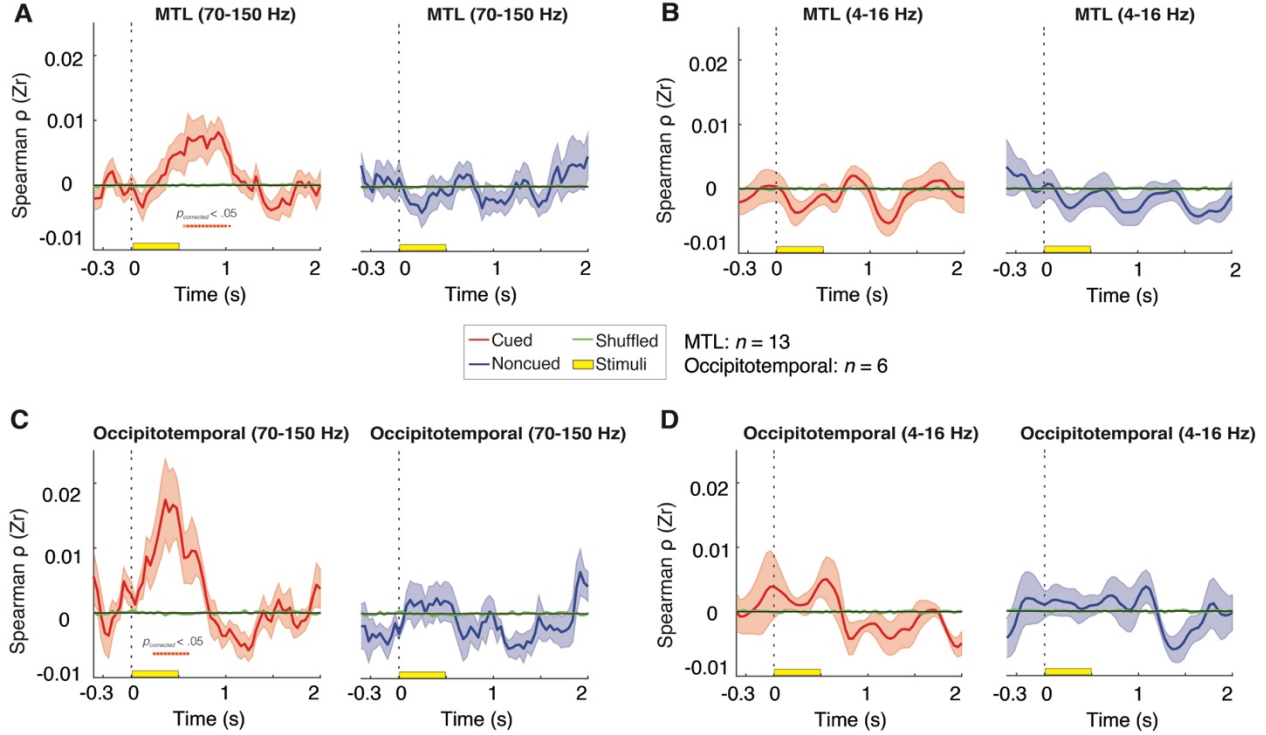


**Fig. S10. Results from representational similarity analysis (RSA) based on high-frequency (70-150 Hz) and low-frequency (4-16 Hz) power patterns in the MTL and occipitotemporal regions in Experiment 3.** At each time point, we calculated the Spearman correlation values (Fisher's Z transformed) between the trial-by-trial stimulus similarity pattern and the neural similarity pattern across trials based on high-frequency power (70-150 Hz) in the MTL (A) and in the occipitotemporal region (C), separately for the cued item (right, red) and uncued item (left, blue). Results from similar analyses based on low-frequency power (4-16 Hz) are plotted in (B) and (D) for the MTL and the occipitotemporal region, respectively. The average results of shuffled-label analyses across participants are plotted in green to establish an empirical chance level. Error areas represent standard errors of mean estimates across participants. The duration when the study items remained on the screen is marked as a yellow bar. Shaded areas represent standard error. \* $p < .05$  after cluster-based correction of family-wise error rate. In summary, we only observed significant item-related variance for the cued item based on high-frequency power in the MTL and in the occipitotemporal regions. No significant association was observed for low-frequency activity.

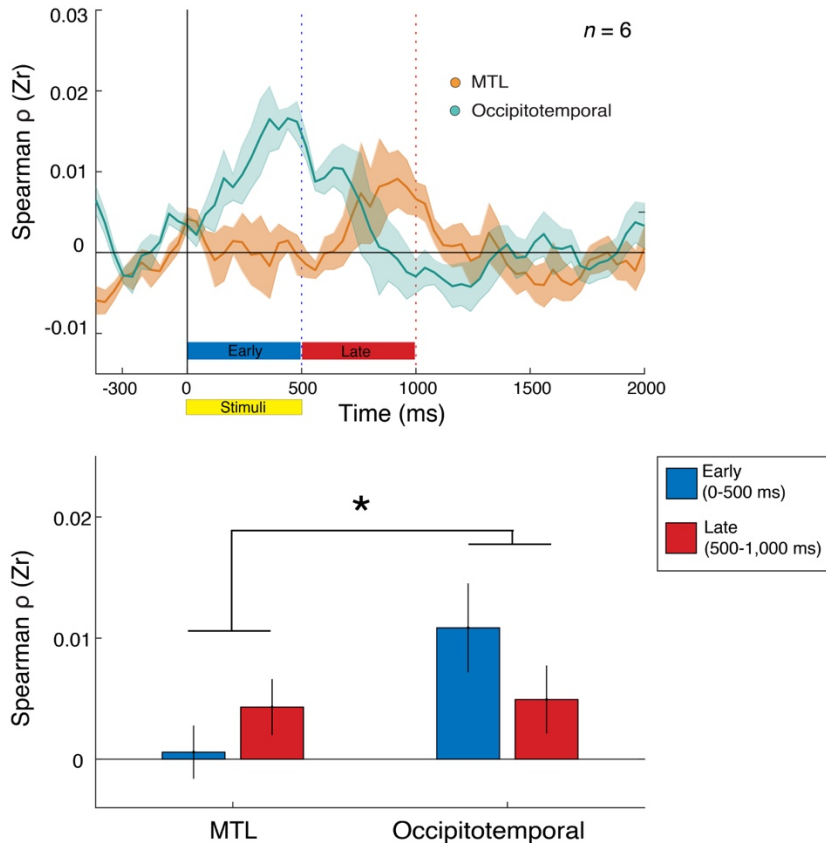


**Fig. S11.** Item-related variance for the cued item in the MTL during WM retention is temporally dissociable from that in the occipitotemporal region during WM encoding in Experiment 3. **(A)** Item-related variances over time for the cued item were plotted separately for the MTL and the occipitotemporal cortex for participants with electrodes in both regions ( $n = 6$ ). We defined two 500 ms time windows during the presentation of the stimuli (marked in yellow) and WM retention interval, namely an early (blue, 0 to 500 ms post-stimulus onset) and a late (red, 500 to 1000 ms post-stimulus onset) time window. Shaded areas around the curve represent standard errors. **(B)** We compared the average item-related variances for the cued item within the early and late time windows in the MTL and the occipitotemporal cortex. We found a significant region by time window interaction effect ( $F(1,5) = 7.39, p = 0.042$ ), while the main effects of the region and time window were not statistically significant ( $p > .25$ ). These results suggest that the MTL's contribution for the retention of precise item-related WM information is temporally separable from occipitotemporal processing of the study items during stimulus presentation. Error bars represent standard errors.

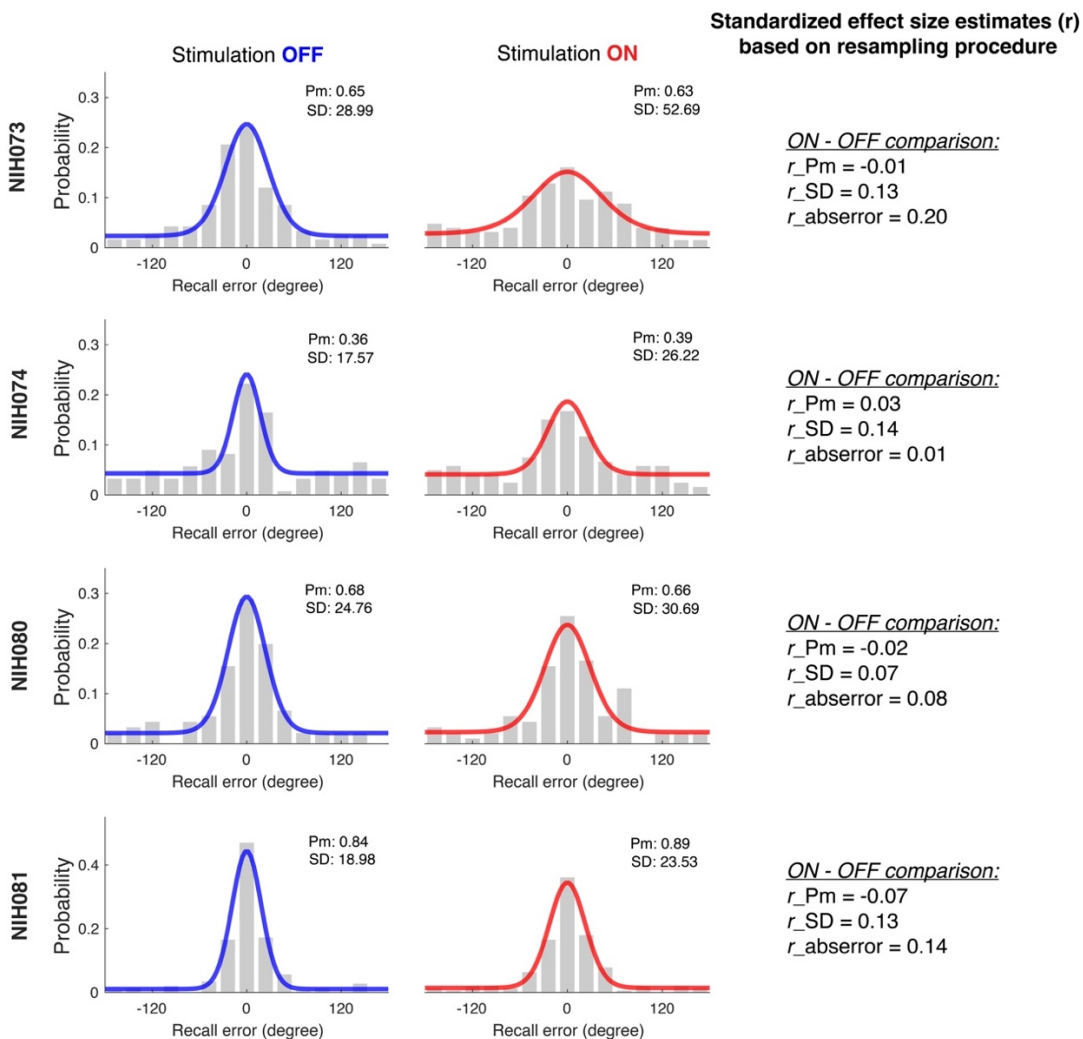


**Fig. S12. Individual best-fit parameters of mixture modeling and effect size estimates ( $r$ -equivalent) in each participant in Experiment 4.** We estimated within-subject effect sizes of parameter difference across stimulation conditions based on resampling  $p$  values across trials (see *Statistical Analysis*) using the  $r$ -equivalent procedure detailed in previous research (71, 78). By combining these standardized effect sizes meta-analytically (70, 71), we found that participants' WM precision was significantly worse (larger recall variability,  $SD$ ) under MTL stimulation as compared with the no stimulation (random effect:  $Zr = 0.12$ , 95% CI: [0.06, 0.19],  $p < .001$ ). In contrast, probability of recall success ( $Pm$ ) was statistically indistinguishable between stimulation and no stimulation conditions (random effect:  $Zr = -0.02$  [-0.08, 0.05],  $p = 0.57$ ), in line with results from the hierarchical Bayesian modeling analysis. Complementarily, we performed a model-free analysis (3) by examining the raw absolute recall errors ( $abserror$ ). We found that absolute recall errors were consistently larger in the stimulation condition, as compared with the no-stimulation condition ( $50.57 \pm 3.38$  vs.  $43.53 \pm 3.73$  degrees) based on the same meta-analysis outlined above (random effect:  $Zr = 0.11$  [0.03, 0.19],  $p = 0.007$ ). Together, both model-free and model-based analyses suggest that participants made more variable errors with MTL stimulation. Here, each row represents data from one participant, separately for the no stimulation condition (blue, left) and the stimulation condition (red, right). Histograms of raw recall errors are plotted into 15 bins (bars), along with the MLE fit (lines).

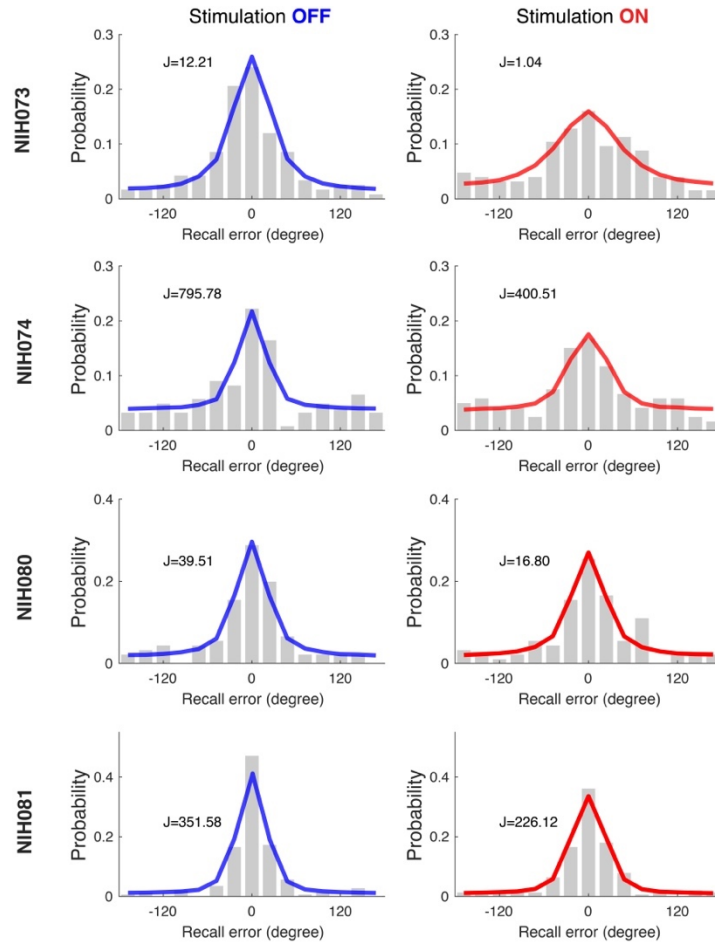


**Fig. S13. Other estimates of WM performance across trials also suggest reduced WM precision under MTL stimulation in Experiment 4.** We also analyzed participants' recall data using the aggregated estimate of variable precision across trials, quantified by Fisher's Information ( $J$ ), assuming no WM capacity limit based on van den Berg and colleagues (4, 79). This measure captures participants' overall WM precision, after taking into account variable precision across trials (see van den Berg and colleagues for the formalization of this measure). We repeated the modeling procedure 100 times for each condition and each subject and used the average  $J$  to quantify participants' WM precision (shown in the figure). The higher the  $J$  value is, the better participants' overall WM precision is (4). For each participant, MTL stimulation markedly decreases the precision of information retained in WM, resulting in a smaller estimate of  $J$ . We also obtained similar precision effects when we consider other models that include additional parameters to account for categorical encoding (29) or mis-binding (80), which are not shown here, but can be replicated via the data available upon request.

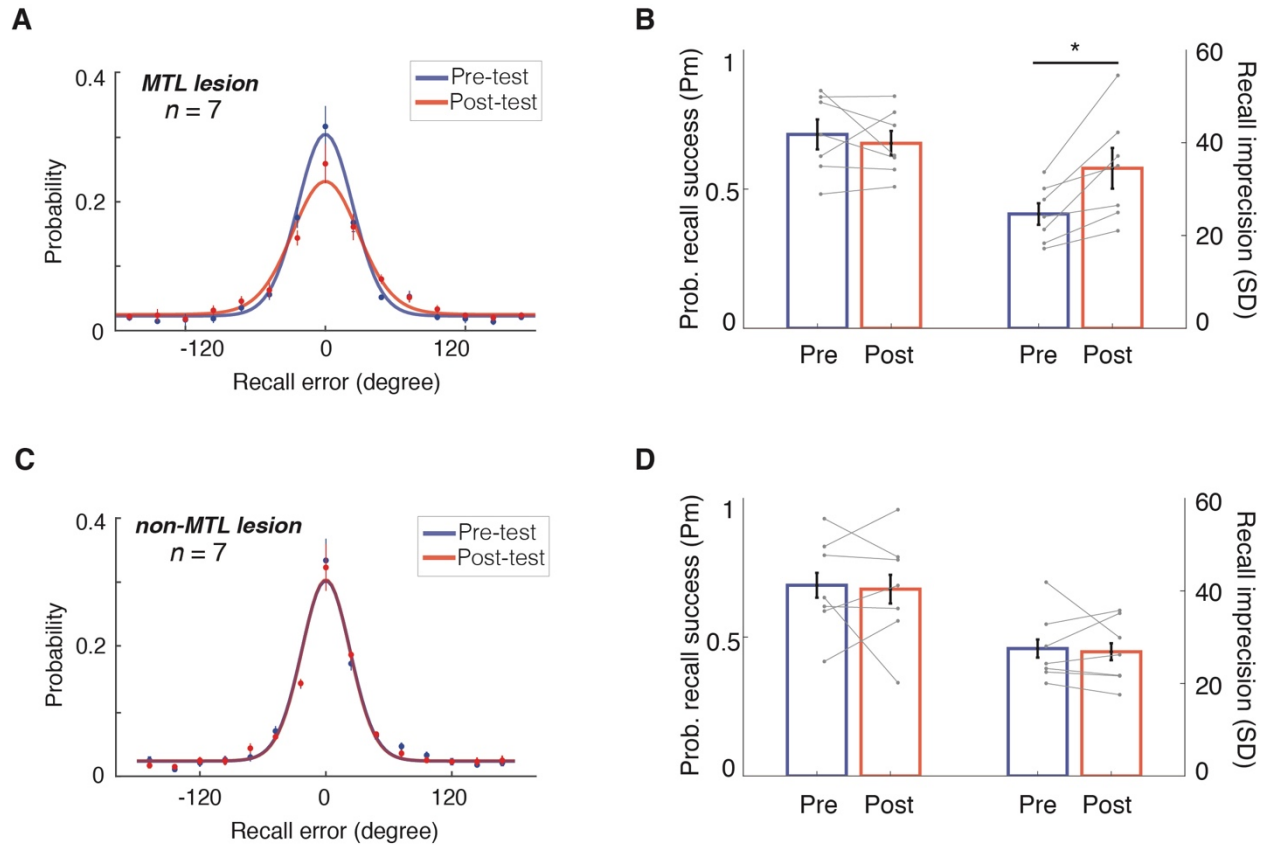


**Fig. S14. Participants' performance in the WM color recall task before and after brain surgery across different lesion groups in Experiment 5.** Recall errors along with Bayesian hierarchical model fits at the group level are shown in (A) and (C) respectively for the MTL-lesion group and non-MTL-lesion group. (B) and (D) summarize individual best-fit Maximal Likelihood Estimation parameters from the mixture model for participants in the MTL-lesion group and non-MTL-lesion group, respectively. Overall, MTL lesions led to markedly increased recall variability (SD) in every participant (B, right y-axis), without significantly affecting the probability of recall success (Pm). However, the participants in the non-MTL-lesion group only showed a minimal difference in either SD or Pm before and after surgery. The effect of surgery on WM precision was greater in the MTL relative to non-MTL group, as supported by a significant interaction effect between testing time points (pre- vs. post-surgery) and lesion groups (MTL vs. non-MTL) in a mixed-effect ANOVA ( $BF_{10} = 81.21$ ;  $F(1,12) = 9.00$ ,  $p = 0.011$ ). Error bars represent standard errors. The fitted lines in (A) and (C) represent best-fit group-level posterior fits from the Bayesian hierarchical modeling procedure. The lines in (B) and (D) represent the mixture model parameters from individual participants across pre- and post-surgical measures.

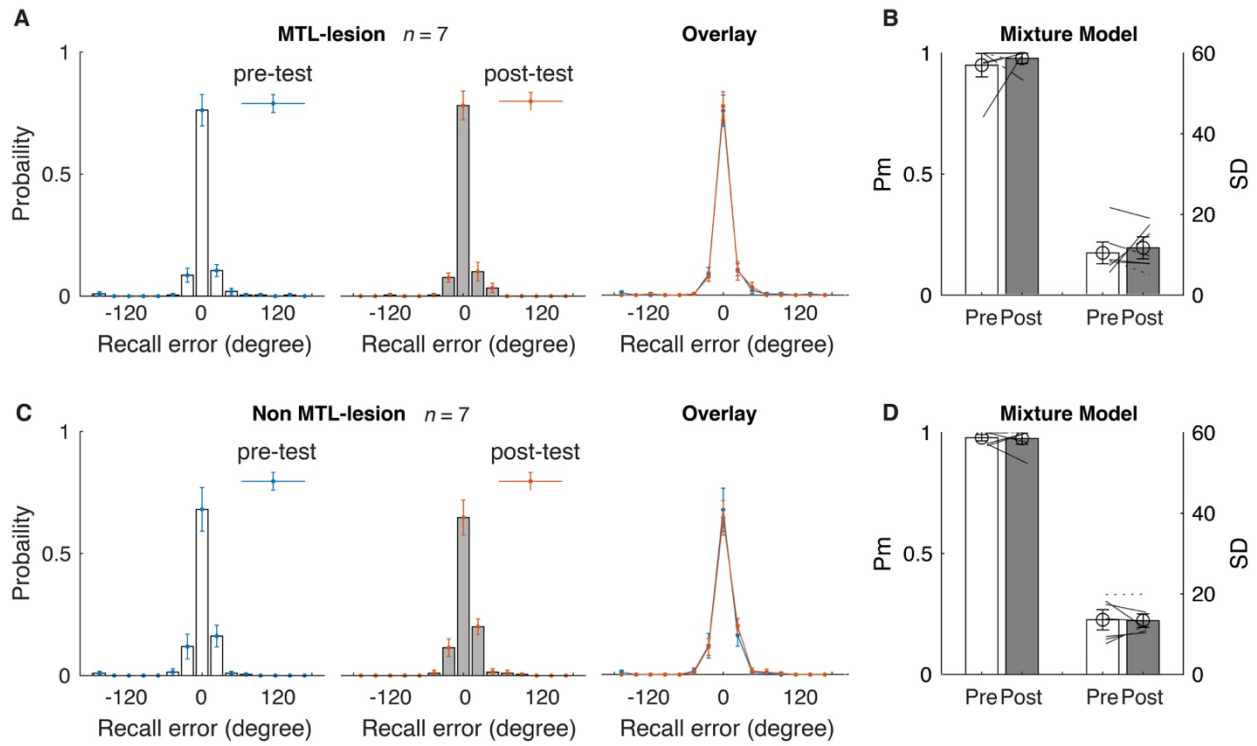


**Fig. S15. Participants' performance in the perceptual/motor control task before and after brain surgery in Experiment 5.** Recall errors from the MTL-lesion group and non-MTL-lesion group are shown in (A) and (C), respectively. (B) and (D) summarize mixture modeling results from the participants in the MTL-lesion group and non-MTL-lesion group, respectively. Overall, participants' performances in this perceptual control task were at the ceiling level, regardless of whether the absolute matching errors or the parameters from the mixture model were compared, before and after brain surgery ( $ts < 1$ ). This is in sharp contrast with the reduced WM precision in MTL-lesion cases after brain surgery. Note, to better visualize the smaller recall errors in this perceptual/motor control task, we did not plot the fitting model lines in (A) and (C). The lines in (B) and (D) represent the mixture model parameters from each individual participant across pre- and post-surgical measures. Error bars represent standard error in these figures.

**Table S1.** Sample size and demographic information of participants in each experiment

Experiments	N	Age (Mean +/- s.e.m.)	Gender (male: female)
Exp. 1	18	22.92 ± 0.87	7:11
Exp. 2	16	21.32 ± 0.73	8:8
Exp. 3*	13	35.85 ± 3.32	8:5
Exp. 4*	4	36.25 ± 8.45	2:2
Exp. 5*	14	36.07 ± 3.32	9:5
Exp. S1	60	19.58 ± 0.24	22:38

*Note.* Exp. = Experiment. \* Experiment 3, 4, and 5 contain overlapping participants. Please see Table S2 for details.

**Table S2. Clinical Characteristics of Each Participant in Experiments 3, 4, and 5**

ID	Age	Sex	IQ	Eth.	Hand.	Lang.	Resection	Exp. 3 (n=13)	Exp. 4 (n=4)	Exp. 5 (n=14)	MTL lesion?
BEH011	37	M	83	W	R	L	left anterior temporal lobectomy and amygdalohippocampectomy			*	Y
BEH012	42	M	89	HS	R	L	left anterior temporal topectomy			*	
BEH013	45	M	NA	AA	R	L	left anterior temporal lobectomy and amygdalohippocampectomy			*	Y
BEH014	19	M	111	W	R	L	right frontal topectomy			*	
BEH015	24	F	77	HS	R	L	right anterior temporal lobectomy and amygdalohippocampectomy			*	Y
NIH064	45	M	78	AS	R	L	right posterior temporal topectomy	*			
NIH065	44	M	89	W	R	L	None	*			
NIH066	24	M	89	HS	R	L	left anterior temporal lobectomy and amygdalohippocampectomy	*			Y
NIH068	36	M	103	W	R	L	left temporal corticectomy and posterior hippocampectomy			*	Y
NIH069	46	F	NA	AA	R	L	None	*		*	
NIH070	34	M	107	W	R	L	right anterior temporal lobectomy and amygdalohippocampectomy	*		*	Y

ID	Age	Sex	IQ	Eth.	Hand.	Lang.	Resection	Exp. 3 (n=13)	Exp. 4 (n=4)	Exp. 5 (n=14)	MTL lesion?
NIH071	57	F	NA	W	R	L	right orbitofrontal cortex, right anterior insula, right temporal lobe			*	
NIH072	33	F	75	HS	R	L	right posterior temporal lobe topectomy	*		*	
NIH073	57	F	73	AA	R	L	None	*	*	*	
NIH074	33	M	74	W	R	L	left anterior temporal lobectomy and amygdalohippocampectomy	*	*	*	Y
NIH075	21	M	87	HS	L	L	left anterior temporal lobectomy and amygdalohippocampectomy	*		*	Y
NIH077	21	M	NA	W	R	L	right frontal topectomy			*	
NIH078	48	F	82	AA	R	L	None	*			
NIH079	26	M	NA	W	R	L	left anterior temporal topectomy of piriform cortex	*			
NIH080	16	F	NA	HS	L	R	left fronto-parietal topectomy	*	*		Y
NIH081	39	M	116	W	R	L	right parietal lesionectomy	*	*		

Note. NA = Not available. Eth. = Ethnicity or Race: W = White, HS = Hispanic, AA = African American, AS = Asian; Hand. = Handedness, Lang. = Language dominance: L = Left, R = Right; Exp. = Experiment, inclusion is marked as \*. Y = Yes.

**Table S3. Electrode contact and trial counts per participant in Experiment 3 and 4.**

	iEEG recording (Experiment 3)				Stimulation (Experiment 4)		
	MTL channel count	OT channel count	Electrode included	Total trials included	No- stimulation trials	Stimulation trials	Total trials included
NIH064	5	10	15	233			
NIH065	14		14	195			
NIH066	6		6	197			
NIH069	5	7	12	209			
NIH070	5	9	14	196			
NIH072	4		4	159			
NIH073	17		17	193	116	124	240
NIH074	8	5	13	226	121	119	240
NIH075	6	7	13	322			
NIH078	7	6	13	194			
NIH079	7		7	232			
NIH080	6		6	262	90	90	180
NIH081	18		18	321	138	138	276
mean	8.31	7.33	11.69	226.08	116.25	117.75	234.00
s.e.m.	1.32	0.52	1.24	13.68	5.51	5.59	19.90

*Note.* MTL = Medial temporal lobe; OT = Occipitotemporal cortex.

**Table S4. Lesion Summary from the neurosurgeon**

MTL related	Resection
BEH011	left anterior temporal lobectomy and amygdalohippocampectomy
BEH013	left anterior temporal lobectomy and amygdalohippocampectomy
BEH015	right anterior temporal lobectomy and amygdalohippocampectomy
NIH068	left temporal corticectomy and posterior hippocampectomy
NIH070	right anterior temporal lobectomy and amygdalohippocampectomy
NIH074	left anterior temporal lobectomy and amygdalohippocampectomy
NIH075	left anterior temporal lobectomy and amygdalohippocampectomy
Non-MTL related	Resection
BEH012	left anterior temporal topectomy
BEH014	right frontal topectomy
NIH069	none
NIH071	right orbitofrontal cortex, right anterior insula, right temporal lobe
NIH072	right posterior temporal lobe topectomy
NIH073	none
NIH077	right frontal topectomy

## References:

1. A. D. Baddeley, *Annu. Rev. Psychol.* **63**, 1–29 (2012).
2. P. M. Bays, M. Husain, *Science* **321**, 851–854 (2008).
3. W. Zhang, S. J. Luck, *Nature* **453**, 233–235 (2008).
4. R. van den Berg, H. Shin, W.-C. Chou, R. George, W. J. Ma, *Proc. Natl. Acad. Sci. U. S. A.* **109**, 8780–8785 (2012).
5. N. Cowan, *Behav. Brain Sci.* **24**, 87–185 (2001).
6. S. J. Luck, E. K. Vogel, *Nature* **390**, 279–281 (1997).
7. S. M. Korkki, F. R. Richter, P. Jeyarathnarajah, J. S. Simons, *Psychol. Aging* **35**, 124–142 (2020).
8. W. Xie, A. Berry, C. Lustig, P. Deldin, W. Zhang, *J. Int. Neuropsychol. Soc.* **25**, 583–594 (2019).
9. E. K. Vogel, M. G. Machizawa, *Nature* **428**, 748–751 (2004).
10. J. J. Todd, R. Marois, *Nature* **428**, 751–754 (2004).
11. T. J. Buschman, M. Siegel, J. E. Roy, E. K. Miller, *Proc. Natl. Acad. Sci. U. S. A.* **108**, 11252–11255 (2011).
12. D. Marr, *Philos. Trans. R. Soc. London B Biol. Sci.* **262**, 23–81 (1971).
13. A. Bakker, C. B. Kirwan, M. Miller, C. E. L. Stark, *Science* **319**, 1640–1642 (2008).
14. M. A. Yassa, C. E. L. Stark, *Trends Neurosci.* **34**, 515–525 (2011).
15. W. B. Scoville, B. Milner, *J. Neurol. Neurosurg. Psychiatry* **20**, 11–21 (1957).
16. J. Kamiński *et al.*, *Nat. Neurosci.* **20**, 590–601 (2017).
17. A. Jeneson, L. R. Squire, *Learn. Mem.* **19**, 15–25 (2012).
18. D. E. Hannula, D. Tranel, N. J. Cohen, *J. Neurosci.* **26**, 8352–8359 (2006).
19. W. Xie, H.-B. Park, K. A. Zaghloul, W. Zhang, *Psychol. Sci.* **31**, 345–348 (2020).
20. P. Wilken, W. J. Ma, *J. Vis.* **4**, 11 (2005).
21. S. M. Stark, M. A. Yassa, J. W. Lacy, C. E. L. Stark, *Neuropsychologia* **51**, 2442–2449 (2013).
22. W. Zhang, S. J. Luck, *Psychol. Sci.* **22**, 1434–1441 (2011).
23. Z. M. Reagh, M. A. Yassa, *Proc. Natl. Acad. Sci. United States Am.* **111**, E4264–E4273 (2014).
24. E. F. Ester, T. C. Sprague, J. T. Serences, *Neuron* **87**, 893–905 (2015).
25. K. C. Bettencourt, Y. Xu, *Nat. Neurosci.* **19**, 150–157 (2015).
26. S. A. Harrison, F. Tong, *Nature* **458**, 632–635 (2009).
27. N. Kriegeskorte, M. Mur, P. Bandettini, *Front. Syst. Neurosci.* **2**, 1–28 (2008).
28. S. Haufe *et al.*, *Neuroimage* **179**, 79–91 (2018).
29. K. O. Hardman, E. Vergauwe, T. J. Ricker, *J. Exp. Psychol. Hum. Percept. Perform.* **43**, 30–54 (2017).
30. W. Zhang, S. J. Luck, *J. Exp. Psychol. Hum. Percept. Perform.* **41**, 22–27 (2015).

31. J. M. Gold *et al.*, *Arch. Gen. Psychiatry*. **67**, 570–577 (2010).
32. W. Xie, W. Zhang, *Emotion*. **16**, 760–774 (2016).
33. T. F. Brady, T. Konkle, J. Gill, A. Oliva, G. A. Alvarez, *Psychol. Sci.* **24**, 981–990 (2013).
34. W. Xie, W. Zhang, *Cognition*. **166**, 73–83 (2017).
35. W. Xie, W. Zhang, *Cogn. Emot.* **32**, 674–690 (2018).
36. W. Xie, W. Zhang, *Mem. Cogn.* **45**, 1423–1437 (2017).
37. K. C. S. Adam, E. K. Vogel, E. Awh, *Cogn. Psychol.* **97**, 79–97 (2017).
38. F. R. Richter, R. A. Cooper, P. M. Bays, J. S. Simons, L. Davachi, *Elife*. **5**, e18260 (2016).
39. M. W. Schurgin, J. T. Wixted, T. F. Brady, *Nat. Hum. Behav.* **4**, 1156–1172 (2020).
40. W. J. Ma, M. Husain, P. M. Bays, *Nat. Neurosci.* **17**, 347–356 (2014).
41. J. C. Lagarias, J. A. Reeds, M. H. Wright, P. E. Wright, *SIAM J. Optim.* **9**, 112–147 (1998).
42. Z. M. Reagh, E. A. Murray, M. A. Yassa, *Hippocampus*. **27**, 169–183 (2017).
43. M. E. Montchal, Z. M. Reagh, M. A. Yassa, *Nat. Neurosci.* **22**, 284–288 (2019).
44. M. O. Irfanoglu *et al.*, *Neuroimage*. **106**, 284–299 (2015).
45. R. W. Cox, *Comput. Biomed. Res.* **29**, 162–173 (1996).
46. H. Wang *et al.*, *IEEE Trans. Pattern Anal. Mach. Intell.* **35**, 611–623 (2015).
47. P. A. Yushkevich *et al.*, *Neuroimage*. **53**, 1208–1224 (2010).
48. G. J. Brouwer, D. J. Heeger, *J. Neurosci.* **29**, 13992–14003 (2009).
49. D. L. Ringach, R. M. Shapley, M. J. Hawken, *J. Neurosci.* **22**, 5639–5651 (2002).
50. T. C. Sprague *et al.*, *eNeuro*. **5**, e0098-18.2018 (2018).
51. P. Kok, P. Mostert, F. P. De Lange, *Proc. Natl. Acad. Sci. U. S. A.* **114**, 10473–10478 (2017).
52. E. F. Ester, A. Nouri, L. Rodriguez, *J. Neurosci.* **38**, 8538–8548 (2018).
53. B. Avants *et al.*, *Acad. Radiol.* **15**, 1360–1375 (2008).
54. N. J. Tustison *et al.*, *Neuroimage*. **99**, 166–179 (2014).
55. M. S. Trotta *et al.*, *Hum. Brain Mapp.* **39**, 709–721 (2017).
56. W. Xie, W. A. Bainbridge, S. K. Inati, C. I. Baker, K. A. Zaghloul, *Nat. Hum. Behav.* **4**, 937–948 (2020).
57. M. X. Cohen, Analyzing Neural Time Series Data (2014).
58. R. M. Furr, R. Rosenthal, *Underst. Stat. Stat. Issues Psychol. Educ. Soc. Sci.* **2**, 33–67 (2003).
59. R. Rosenthal, R. L. Rosnow, D. B. Rubin, *Contrasts and Effect Sizes in Behavioral Research: A Correlational Approach* (Cambridge University Press, New York, NY, US, 2000).
60. J. Williams, D. P. MacKinnon, *Struct. Equ. Model. A Multidiscip. J.* **15**, 23–51 (2008).
61. J. Kruschke, *Doing Bayesian Data Analysis* (Academic Press, Cambridge, MA, 2015).

62. J. N. Rouder, J. Lu, *Psychon. Bull. Rev.* **12**, 573–604 (2005).
63. T. Sorensen, S. Hohenstein, S. Vasishth, *Quant. Methods Psychol.* **12**, 175–200 (2016).
64. E.-J. Wagenmakers, T. Lodewyckx, H. Kuriyal, R. Grasman, *Cogn. Psychol.* **60**, 158–189 (2010).
65. E. J. Wagenmakers, R. D. Morey, *Curr. Dir. Psychol. Sci.* **25**, 169–176 (2016).
66. B. Carpenter *et al.*, *J. Stat. Softw.* **76**, 1–32 (2017).
67. P. C. Bürkner, *J. Stat. Softw.* **80**, 1–27 (2017).
68. A. F. Jarosz, J. Wiley, *J. Probl. Solving* **7**, 1–8 (2014).
69. J. N. Rouder, J. M. Haaf, J. Vandekerckhove, *Psychon. Bull. Rev.* **25**, 102–113 (2018).
70. R. Rosenthal, M. R. DiMatteo, *Annu. Rev. Psychol.* **52**, 59–82 (2001).
71. W. Xie, M. Cappiello, M. Meng, R. Rosenthal, W. Zhang, *Neurosci. Biobehav. Rev.* **92**, 402–416 (2018).
72. S. Kornblith, R. Quian Quiroga, C. Koch, I. Fried, F. Mormann, *Curr. Biol.* **27**, 1026–1032 (2017).
73. E. Boran *et al.*, *Sci. Adv.* **5**, eaav3687 (2019).
74. T. C. Sprague, E. F. Ester, J. T. Serences, *Neuron* **91**, 694–707 (2016).
75. E. F. Ester, D. E. Anderson, J. T. Serences, E. Awh, *J. Cogn. Neurosci.* **25**, 754–761 (2013).
76. N. Kriegeskorte, R. Goebel, P. Bandettini, *Proc. Natl. Acad. Sci. United States Am.* **103**, 3863–3868 (2006).
77. M. J. Wolff, J. Ding, N. E. Myers, M. G. Stokes, *Front. Syst. Neurosci.* **9**, 1–12 (2015).
78. R. Rosenthal, D. B. Rubin, *Psychol. Methods* **8**, 492–496 (2003).
79. R. van den Berg, E. Awh, W. J. Ma, *Psychol. Rev.* **121**, 124–149 (2014).
80. P. M. Bays, R. F. G. Catalao, M. Husain, *J. Vis.* **9**, 7–7 (2009).